Vertical structure and physical processes of the Madden-Julian oscillation: exploring key model physics in climate simulations

AGU PUBLICATIONS

JGR

Journal of Geophysical Research: Atmospheres

RESEARCH ARTICLE
10.1002/2014JD022375

This article is a companion to *Klingaman et al.* [2015a] doi:10.1002/2014JD022374; *Xavier et al.* [2015] doi:10.1002/2014JD022718; and *Klingaman et al.* [2015b] doi:10.1002/2015JD023196.

Key Points:
- Realistic vertical structure is closely related to good MJO simulations
- Environment moisture and convection-circulation feedback are critical for MJO
- Air-sea interaction can significantly improve MJO simulations in many GCMs

Correspondence to:
X. Jiang,
xianan@ucla.edu

Citation:
Jiang, X., et al. (2015), Vertical structure and physical processes of the Madden-Julian oscillation: Exploring key model physics in climate simulations, *J. Geophys. Res. Atmos.*, *120*, 4718–4748, doi:10.1002/2014JD022375.

Received 5 AUG 2014
Accepted 6 APR 2015
Accepted article online 10 APR 2015
Published online 26 MAY 2015

Vertical structure and physical processes of the Madden-Julian oscillation: Exploring key model physics in climate simulations

Xianan Jiang[1,2], Duane E. Waliser[1,2], Prince K. Xavier[3], Jon Petch[3], Nicholas P. Klingaman[4], Steven J. Woolnough[4], Bin Guan[1,2], Gilles Bellon[5], Traute Crueger[6], Charlotte DeMott[7], Cecile Hannay[8], Hai Lin[9], Wenting Hu[10], Daehyun Kim[11], Cara-Lyn Lappen[12], Mong-Ming Lu[13], Hsi-Yen Ma[14], Tomoki Miyakawa[15], James A. Ridout[16], Siegfried D. Schubert[17], John Scinocca[18], Kyong-Hwan Seo[19], Eiki Shindo[20], Xiaoliang Song[21], Cristiana Stan[22], Wan-Ling Tseng[23], Wanqiu Wang[24], Tongwen Wu[25], Xiaoqing Wu[26], Klaus Wyser[27], Guang J. Zhang[21], and Hongyan Zhu[28]

[1]Joint Institute for Regional Earth System Science and Engineering, University of California, Los Angeles, California, USA, [2]Jet Propulsion Laboratory, California Institute of Technology, Pasadena, California, USA, [3]UK Met Office, Exeter, UK, [4]National Centre for Atmospheric Science and Department of Meteorology, University Reading, Reading, UK, [5]CNRM-GAME, Centre National de la Recherche Scientifique/Météo-France, Toulouse, France, [6]Max Planck Institute for Meteorology, Hamburg, Germany, [7]Department of Atmospheric Science, Colorado State University, Fort Collins, Colorado, USA, [8]National Center for Atmospheric Research, Boulder, Colorado, USA, [9]Environment Canada, Dorval, Quebec, Canada, [10]State Key Laboratory of Numerical Modeling for Atmospheric Sciences and Geophysical Fluid Dynamics, Institute of Atmospheric Physics, Chinese Academy of Sciences, Beijing, China, [11]Lamont-Doherty Earth Observatory, Columbia University, New York, New York, USA, [12]Department of Atmospheric Science, Texas A&M University, College Station, Texas, USA, [13]Central Weather Bureau, Taipei, Taiwan, [14]Lawrence Livermore National Laboratory, Livermore, California, USA, [15]Department of Coupled Ocean-Atmosphere-Land Processes Research, Japan Agency for Marine-Earth Science and Technology, Yokosuka, Japan, [16]Naval Research Laboratory, Monterey, California, USA, [17]Global Modeling and Assimilation Office, NASA GSFC, Greenbelt, Maryland, USA, [18]Canadian Centre for Climate Modelling and Analysis, Environment Canada, Victoria, British Columbia, Canada, [19]Department of Atmospheric Sciences, Pusan National University, Pusan, South Korea, [20]Climate Research Department, Meteorological Research Institute, Tsukuba, Japan, [21]Scripps Institute of Oceanography, La Jolla, California, USA, [22]Department of Atmospheric, Oceanic and Earth Sciences, George Mason University, Fairfax, Virginia, USA, [23]University Research Center for Environmental Changes, Academia Sinica, Taipei, Taiwan, [24]Climate Prediction Center, National Centers for Environmental Prediction/NOAA, Camp Springs, Maryland, USA, [25]Beijing Climate Center, China Meteorological Administration, Beijing, China, [26]Department of Geological and Atmospheric Sciences, Iowa State University, Ames, Iowa, USA, [27]Rossby Centre, Swedish Meteorological and Hydrological Institute, Norrkoping, Sweden, [28]Centre for Australian Weather and Climate Research, Bureau of Meteorology, Melbourne, Victoria, Australia

Abstract Aimed at reducing deficiencies in representing the Madden-Julian oscillation (MJO) in general circulation models (GCMs), a global model evaluation project on vertical structure and physical processes of the MJO was coordinated. In this paper, results from the climate simulation component of this project are reported. It is shown that the MJO remains a great challenge in these latest generation GCMs. The systematic eastward propagation of the MJO is only well simulated in about one fourth of the total participating models. The observed vertical westward tilt with altitude of the MJO is well simulated in good MJO models but not in the poor ones. Damped Kelvin wave responses to the east of convection in the lower troposphere could be responsible for the missing MJO preconditioning process in these poor MJO models. Several process-oriented diagnostics were conducted to discriminate key processes for realistic MJO simulations. While large-scale rainfall partition and low-level mean zonal winds over the Indo-Pacific in a model are not found to be closely associated with its MJO skill, two metrics, including the low-level relative humidity difference between high- and low-rain events and seasonal mean gross moist stability, exhibit statistically significant correlations with the MJO performance. It is further indicated that increased cloud-radiative feedback tends to be associated with reduced amplitude of intraseasonal variability, which is incompatible with the radiative instability theory previously proposed for the MJO. Results in this study confirm that inclusion of air-sea interaction can lead to significant improvement in simulating the MJO.

1. Introduction

Since its discovery in the 1970s by the pioneering work of *Madden and Julian* [1971, 1972], the significant role of the Madden-Julian oscillation (MJO) for tropical atmospheric variability has been widely recognized (see reviews by *Lau and Waliser* [2012], *Zhang* [2013], and *Serra et al.* [2014]). The MJO exerts pronounced modulations on global climate and weather, including monsoons [e.g., *Yasunari*, 1979, 1980; *Lau and Chan*, 1986; *Sperber et al.*, 2000; *Annamalai and Sperber*, 2005; *Lorenz and Hartmann*, 2006; *Wheeler et al.*, 2009; *Sultan et al.*, 2003], tropical cyclone activity [e.g., *Nakazawa*, 1988; *Liebmann et al.*, 1994; *Maloney and Hartmann*, 2000; *Bessafi and Wheeler*, 2006; *Klotzbach*, 2010; *Jiang et al.*, 2012], tropical convectively coupled waves [*Kiladis et al.*, 2009; *Serra et al.*, 2014], and diurnal convective events [*Rauniyar and Walsh*, 2011; *Oh et al.*, 2012; *Virts et al.*, 2013]. In addition to the tropics, widespread influences by the MJO have also been detected over extratropical regions through emanation of Rossby waves (e.g., *Vecchi and Bond* [2004], *Cassou* [2008], *L'Heureux and Higgins* [2008], *Lin et al.* [2009], *Guan et al.* [2012], *Seo and Son* [2012], and many others). On the other hand, the collective influence of surface winds associated with the MJO may trigger or terminate El Niño/Southern Oscillation events [e.g., *Takayabu et al.*, 1999; *McPhaden*, 1999; *Kessler and Kleeman*, 2000; *Hendon et al.*, 2007]. In light of its prominent role in bridging weather and climate, the quasi-periodically occurring MJO on intraseasonal time scales represents one of the primary predictability sources for extended-range weather prediction [e.g., *Waliser*, 2012; *Gottschalck et al.*, 2010; *National Academy of Sciences*, 2010], filling a gap between deterministic weather forecast and climate prediction. This also provides a critical basis for the recently advocated “seamless prediction” concept [*Hurrell et al.*, 2009; *Brown et al.*, 2012].

While great progress has been achieved in the development of general circulation models (GCMs) in recent decades, the MJO, however, still remains poorly represented in these state-of-the-art GCMs, even in their latest versions [e.g., *Kim et al.*, 2009; *Hung et al.*, 2013]. Meanwhile, our predictive skill for the MJO remains limited, with a typical scale of 2–3 weeks [*Seo et al.*, 2009; *Vitart and Molteni*, 2010; *Rashid et al.*, 2011; *Wang et al.*, 2013; *Neena et al.*, 2014], in contrast to its intrinsic predictability of about 4–5 weeks [*Waliser et al.*, 2003; *Ding et al.*, 2010; *Neena et al.*, 2014]. As GCMs are essential tools for projection of future climate changes, large model deficiencies in depicting this fundamental form of atmospheric variability leave us greatly disadvantaged in undertaking climate change studies, particularly in projecting future activities of extreme events that are significantly modulated by the MJO.

The great challenges in simulating and predicting the MJO that we are facing indicate that our knowledge of the fundamental physics of the MJO is still elusive. In interpreting instability and eastward propagation of the observed MJO, existing MJO theories have been largely built upon the observed vertical tilting structures in moisture and diabatic heating fields associated with the MJO. Enhanced lower tropospheric moisture anomalies were observed to first appear at the eastern edge of the MJO convection [e.g., *Kemball-Cook and Weare*, 2001; *Sperber*, 2003; *Kiladis et al.*, 2005; *Tian et al.*, 2010], coupled with planetary boundary layer (PBL) convergence [*Sperber*, 2003; *Kiladis et al.*, 2005], and shallow heating structure [e.g., *Lin et al.*, 2004; *Kiladis et al.*, 2005] along with shallow cumuli/congestus clouds [*Johnson et al.*, 1999; *Kikuchi and Takayabu*, 2004; *Chen and Del Genio*, 2009; *Tromeur and Rossow*, 2010]. This coupling between shallow convection and circulation in the PBL is considered a key preconditioning process in driving the eastward movement of the MJO, which has also been supported by GCM studies [e.g., *Zhang and Mu*, 2005a; *Benedict and Randall*, 2009; *Li et al.*, 2009; *Zhang and Song*, 2009; *Cai et al.*, 2013; *Lappen and Schumacher*, 2014].

Different physical processes have been ascribed to this MJO preconditioning process, including through ocean surface flux [*Emanuel*, 1987; *Neelin et al.*, 1987; *Maloney and Sobel*, 2004; *Sobel et al.*, 2010], PBL convergence or vertical motion through a “Frictional CISK (Convective Instability of the Second Kind)” [*Salby et al.*, 1994; *Wang and Li*, 1994; *Maloney and Hartmann*, 1998; *Hsu and Li*, 2012], moisture transport [e.g., *Maloney*, 2009; *Maloney et al.*, 2010; *Andersen and Kuang*, 2012; *Hsu and Li*, 2012], cloud water detrainment/evaporation from shallow cumuli/congestus clouds [*Johnson et al.*, 1999; *Ruppert and Johnson*, 2014], and air-sea interaction [*Waliser et al.*, 1999; *Kemball-Cook and Wang*, 2001; *Sperber et al.*, 2005; *Klingaman and Woolnough*, 2014; *DeMott et al.*, 2014].

In addition to the interaction between shallow convection and circulation, other theoretical and modeling work also emphasized the role of stratiform heating in destabilizing the MJO deep convection. The positive covariance between the second baroclinic modes of heating and temperature anomalies could lead to the generation of eddy available potential energy (EAPE), and thus amplify the MJO disturbance [e.g., *Fu and Wang*, 2009; *Seo and Wang*, 2010; *Holloway et al*., 2013], similar to the "stratiform-instability" concept proposed for convectively coupled equatorial waves (CCEWs) [*Mapes*, 2000; *Khouider and Majda*, 2006; *Majda and Biello*, 2004; *Kuang*, 2008]. On the other hand, reduced longwave radiative cooling during enhanced MJO convection, evident in recent satellite estimates[*Jiang et al*., 2011; *Ma and Kuang*, 2011], could also play a critical role for growth of the MJO ("radiative instability") [*Raymond*, 2001; *Lee et al*., 2001; *Sobel and Gildor*, 2003; *Bony and Emanuel*, 2005; *Lin and Mapes*, 2004; *Lin et al*., 2007; *Andersen and Kuang*, 2012].

While different heating components have been emphasized in the above MJO theories, recent observational studies, however, are not consistent in their findings regarding the vertical heating structure of the MJO. The transition from a shallow heating, to deep, and then to top-heavy stratiform heating structure during the MJO evolution, has been reported based on field campaign observations [*Lin et al*., 2004; *Kiladis et al*., 2005] and recent reanalysis data sets [*Jiang et al*., 2011; *Ling and Zhang*, 2011]. This vertical tilt in MJO heating, however, was not clearly evident in sounding observations during the *Mirai* Indian Ocean Cruise for the Study of the MJO Convection Onset field experiment [*Katsumata et al*., 2009] or in estimates based on TRMM (Tropical Rainfall Measuring Mission) and the International Satellite Cloud Climatology Project, particularly over the Indian Ocean [*Morita et al*., 2006; *Jiang et al*., 2009; *Zhang et al*., 2010; *Ling and Zhang*, 2011; *Jiang et al*., 2011; *Stachnik et al*., 2013]. While the controversy in MJO vertical structure could arise in part from the sampling of MJO events, location of the observations (Indian Ocean versus western Pacific), or deficiencies in satellite-based heating estimates [e.g., *Berg et al*., 2010; *Jiang et al*., 2011], it necessitates further investigations on the key vertical structure and associated processes of the MJO.

Most recently, there have been interesting developments in understanding the essence of the MJO, including a school of thought that regards the MJO as a "moisture mode" [*Raymond*, 2001; *Raymond and Fuchs*, 2009; *Sugiyama*, 2009; *Sobel and Maloney*, 2012; *Sobel and Maloney*, 2013]. The critical basis for this hypothesis is that under the weak temperature gradient approximation, as for the Indo-Pacific region where the MJO exhibits the strongest amplitude, the fundamental dynamics of the dominant mode are controlled by processes associated with tropospheric moisture, rather than wave dynamics [*Sobel et al*., 2001; *Raymond*, 2001]. This moisture mode theory predicts that convective activity exhibits great sensitivity to atmospheric moisture, which is supported by observations [*Bretherton et al*., 2004; *Peters and Neelin*, 2006; *Holloway and Neelin*, 2009; *Thayer-Calder and Randall*, 2009; *Sahany et al*., 2012]. Meanwhile, modeling studies have demonstrated that increasing the constraints on convection by column moisture can indeed lead to the improvement of MJO simulations [*Tokioka et al*., 1988; *Bechtold et al*., 2008; *Zhu et al*., 2009; *Chikira and Sugiyama*, 2010; *Hannah and Maloney*, 2011; *Hagos et al*., 2011; *Kim et al*., 2012]. Motivated by these observational and modeling studies, metrics measuring convection-moisture sensitivity have been recently explored to discriminate key processes for good and poor MJO simulations across multiple GCMs [*Kim et al*., 2014b ; *Maloney et al*., 2014]. Results have suggested that models that exhibit larger contrast in lower tropospheric humidity between heavy and light rain events tend to produce better MJO simulations.

To identify essential processes responsible for destabilization and propagation of the MJO, various moist static energy (MSE) sources and sinks have been examined in depth [e.g., *Maloney*, 2009; *Maloney et al*., 2010; *Andersen and Kuang*, 2012; *Hsu and Li*, 2012; *Cai et al*., 2013; *Wu and Deng*, 2013]. In order to depict the efficiency with which convection and associated divergent circulations discharge moisture in the atmosphere column, the original concept of "gross moist stability (GMS)" was developed by *Neelin and Held* [1987], which was defined as net vertical MSE export per unit vertical mass flux. The GMS was further generalized to also include the effects of horizontal advection [*Raymond and Fuchs*, 2009; *Raymond et al*., 2009]. Based on the moisture mode theory, the circulation induced by the MJO convection must act to further moisten the atmosphere. For such moistening to occur, a negative value of the GMS, or effective GMS if combined with effects from external forcing including surface heat fluxes and radiative heating, is needed to maintain an unstable mode [*Raymond et al*., 2009; *Sobel and Maloney*, 2013]. Improved simulations of the MJO or boreal summer intraseasonal variability over the eastern Pacific associated with lower GMS have been demonstrated in recent GCM studies [*Hannah and Maloney*, 2011; *Benedict et al*., 2014; *Pritchard and Bretherton*, 2014; *Maloney et al*., 2014].

In light of the essential role of diabatic heating and related moist processes in MJO physics, and a goal toward improvement of model capabilities in representing the MJO, it is of great interest to comprehensively characterize vertical structure of diabatic processes associated with the MJO and explore how their structures and fidelity relate to the models' MJO representation and forecast skill. With this in mind, the MJO Task Force (MJOTF), under the auspices of YOTC (the "Year" of Tropical Convection) [*Moncrieff et al*., 2012; *Waliser et al*., 2012], and the GEWEX Atmospheric System Study (GASS) developed a modeling experiment to help address the above objectives [*Petch et al*., 2011]. (Note that the MJOTF was recently reformulated and now is under the auspices of the Working Group on Numerical Experimentation, WGNE).

In this manuscript, details of this MJOTF/GASS MJO model evaluation project will be introduced. Results obtained from this project will be reported with a particular focus on the climate simulation component. The outline of this paper is as follows. In section 2, details of the project, including experiment designs of the three components, will be introduced. Additionally, participating models for the climate simulation component, as well as the observational data sets to be analyzed for this study, will also be briefly described in this section. Evaluation of the general performances in representing the MJO in participating model simulations will be given in section 3. In section 4, several process-oriented metrics will be explored. Composite vertical structures associated with the MJO in models with good and poor MJO will be further illustrated in section 5. A summary and a discussion are presented in section 6.

2. Experiment Design, Participating Models, and Observational Data Sets

2.1. Experiment Design of the MJOTF/GASS Global MJO Model Comparison Project

The MJOTF/GASS MJO global model comparison project consists of three experimental components, including (a) a 20 year climate simulation, (b) a 2 day hindcast, and (c) a 20 day hindcast component. The design of these three components was mainly motivated by the known links between model biases in long-term climate simulations and short-range forecasts [*Phillips et al*., 2004]. Clues on the key deficiencies in representing the MJO in a climate model could be gained by examining the processes based on short-term forecasts of the same model [e.g., *Boyle et al*., 2008; *Xie et al*., 2012; *Ma et al*., 2013]. While details of and results from the two hindcast components will be covered in two companion papers: [*Xavier et al*., 2015] for the 2 day hindcast component and [*Klingaman et al*., 2015a] for the 20 day hindcast component, in this study we mainly focus on the 20 year climate simulation component of this project.

For the 20 year climate simulation component, participating models, either with an atmospheric-only GCM (AGCM) or an atmosphere-ocean coupled system or both, were integrated for 20 years. For AGCM runs, weekly sea surface temperatures (SST) and sea ice concentrations based on the NOAA Optimum Interpolation V2 product [*Reynolds et al*., 2002] for the 20 year period of 1991–2010 were specified as the model lower boundary conditions. Output from all the participating GCMs was archived at every 6 h on standard horizontal (2.5° × 2.5°) grids and 22 vertical pressure levels. This component aims to characterize the capability of a model in representing the intrinsic MJO variability and to explore key processes responsible for a high-quality representation of the MJO.

Output from all models includes 3-D variables such as winds (u, v), temperature (T), specific (q) and relative humidity, and also 2-D variables including rainfall and surface flux terms etc., as well as budget terms of u, v, T, and q, which provide an excellent opportunity to characterize detailed source and sink processes of moisture, heat, and momentum associated with the MJO. For more details about this project and a complete list of variables archived from participating GCMs in the three components, readers are referred to the project website: http://www.ucar.edu/yotc/mjodiab.html.

2.2. Participating Models in the 20 Year Climate Simulation Component

A list of models participating in the 20 year climate simulation component, along with horizontal and vertical resolutions used in each model, is given in Table 1. For detailed documentation of physical parameterization schemes adopted in these models, please refer to corresponding references. There are 27 simulations from 24 GCMs in this component. A majority of these models are based on a conventional parameterization approach in depicting cumulus processes except two experiments, SPCCSM3 and SPCAM3. These experiments were based on the National Center for Atmospheric Research (NCAR) Community Atmosphere Model (CAM) with the "superparameterization" technique, in which a 2-D cloud-resolving model is embedded within each grid box of the host model to replace the conventional cumulus

Table 1. Participating Models With Horizontal/Vertical Resolutions

	Model Name	Institute	Horizontal Resolution (Lon × Lat), Vertical Levels	References
1	ACCESS1	*Centre for Australian Weather and Climate Research*	1.875° × 1.25°, L85	*Zhu et al.* [2013]
2	BCC-AGCM2.1	*Beijing Climate Center, China Meteorological Administration*	T42 (2.8), L26	*Wu et al.* [2010]
3	CAM5	*National Center for Atmospheric Research*	1.25° × 0.9°, L30	*Neale et al.* [2012]
4	CAM5-ZM	*Lawrence Livermore National Laboratory*	1.25° × 0.9°, L30	*Song and Zhang* [2011]
5	CanCM4*	*Canadian Centre for Climate Modelling and Analysis*	2.8°, L35	*Merryfield et al.* [2013]
6	CFS2	*Climate Prediction Center, NCEP/NOAA*	T126 (1°), L64	*Saha et al.* [2013]
7a	CNRM-AM	*Centre National de la Recherche Scientifique/Météo-France*	T127(1.4), L31	*Voldoire et al.* [2013]
7b	CNRM-CM*			
7c	CNRM-ACM			
8	CWB-GFS	*Central Weather Bureau, Taiwan*	T119 (1°), L40	*Liou et al.* [1997]
9	ECEarth3	*Rossby Centre, Swedish Meteorological and Hydrological Institute*	T255 (80 km), L91	see note[a]
10	EC-GEM	*Environment Canada*	1.4°, L64	*Côté et al.* [1998]
11	ECHAM5-SIT*	*Academia Sinica, Taiwan*	T63 (2°), L31	*Tseng et al.* [2014]
12	ECHAM6*	*Max Planck Institute for Meteorology*	T63 (2°), L47	*Stevens et al.* [2013]
13	FGOALS-s2	*Institute of Atmospheric Physics, Chinese Academy of Sciences*	R42 (2.8° × 1.6°), L26	*Bao et al.* [2013]
14	GEOS5	*Global Modeling and Assimilation Office, NASA*	0.625° × 0.5°, L72	*Molod et al.* [2012]
15	GISS-E2	*Goddard Institute for Space Studies, NASA*	2.5° × 2.0°, L40	*Schmidt et al.* [2014]
16	ISUGCM	*Iowa State University*	T42 (2.8°), L18	*Wu and Deng* [2013]
17	MetUM-GA3	*U. K. Met Office*	1.875° × 1.25°, L85	*Walters et al.* [2011]
18	MIROC5	*AORI/NIES/JAMSREC, Japan*	T85 (1.5°), L40	*Watanabe et al.* [2010]
19	MRI-AGCM3	*Meteorological Research Institute, Japan*	T159, L48	*Yukimoto et al.* [2012]
20	NavGEM1	*US Naval Research Laboratory*	T359 (37 km), L42	see note[b]
21	PNU-CFS*	*Pusan National University*	T62 (2°), L64	*Saha et al.* [2006]
22a	SPCAM3	*Colorado State University*	T42 (2.8°), L30	*Khairoutdinov et al.* [2008]
22b	SPCCSM3*	*George Mason University*	T42 (2.8°), L30	*Stan et al.* [2010]
23	TAMU-CAM4	*Texas A&M University*	2.5° × 1.9°, L26	*Lappen and Schumacher* [2012]
24	UCSD-CAM3	*Scripps Institute of Oceanography*	T42 (2.8°), L26	*Zhang and Mu* [2005b]

[a] *Hazeleger et al.* [2012] describes an earlier version of the EC-EARTH model, while here we have used a newer version based on ECMWF's IFS model cy36r4. The main differences between these model versions are an improved radiation scheme [*Morcrette et al.*, 2008] and a new cloud microphysics [*Forbes et al.*, 2012].
[b] The NAVGEM version 1.0 model used here, for which there is no published reference, differs from NAVGEM 1.1 [*Hogan et al.*, 2014] in that it lacks prognostic cloud water and that it uses the radiation scheme of *Harshvardhan et al.* [1987].

parameterizations [*Randall et al.*, 2003]. While SPCAM3 is an atmospheric-only version of the superparameterized model built on the version 3 of the CAM (CAM3) [*Khairoutdinov et al.*, 2008], SPCCSM3 is a coupled run based on the same AGCM [*Stan et al.*, 2010]. It has been reported that much improved MJO simulations can be achieved in these superparameterized GCMs [e.g., *Benedict and Randall*, 2007; *Stan et al.*, 2010; *DeMott et al.*, 2011]. While most of the contributions to the climate simulation component were conducted with an AGCM configuration, there are five other coupled GCM (CGCM) runs in addition to the SPCCSM3 (denoted by an asterisk by the model name in Table 1). Also noteworthy is that three simulations were conducted based on the CNRM GCM, including an AGCM integration forced by the observed weekly SST and sea ice (CNRM-AM), a CGCM run (CNRM-CM), and a third experiment in which the AGCM was forced by the monthly mean SST and sea ice output from the coupled run (CNRM-ACM). Since the atmospheric model used for these three integrations was the same, these experiments provide an excellent opportunity to explore how interactive processes at the atmosphere and ocean interface can improve MJO simulations.

In addition to the SPCCSM3 and SPCAM3 mentioned above, there are several other simulations based on different versions and/or modifications of the NCAR CAM model, including NCAR CAM5 (v5), UCSD-CAM3 (v3), TAMU-CAM4 (v4), ISUGCM (v3), and CAM5-ZM (v5). Particularly noteworthy is the TAMU-CAM4, in which the "observed" latent heating structure for the MJO based on TRMM estimates was used to constrain both the horizontal and vertical distribution of model heating throughout the tropics [*Lappen and Schumacher*, 2012]. It was found that the model MJO is significantly improved over the original CAM after applying this technique, which is also to be illustrated in the following analyses, further suggesting the critical role of the vertical heating structure for realistic simulations of the MJO.

2.3. Observational Data Set

The primary observational data sets used for this analysis include TRMM-based rainfall observations (version 3B42 v7) [*Huffman et al.*, 1995] and the European Center for Medium-Range Weather Forecasting (ECMWF) ERA-Interim reanalysis [*Dee et al.*, 2011] for the period of 1998–2012. TRMM 3B42 rainfall is a global precipitation product based on multisatellite and rain gauge analysis. It provides precipitation estimates with 3-hourly temporal resolution on a 0.25° spatial resolution in a global belt extending from 50°S to 50°N. With a horizontal resolution of 1.5° × 1.5°, the ERA-Interim reanalysis provides daily 3-D profiles of temperature, specific and relative humidity, *u* and *v* winds, and pressure vertical velocity. Both the raw TRMM rainfall and ERA-Interim reanalysis data are interpolated onto the same grids as the GCM output, i.e., 2.5° × 2.5° at 22 standard vertical pressure levels.

3. Evaluation of MJO Simulated in GCMs

In this study, we mainly focus our analyses on the MJO during the boreal winter season from November to April, when it is largely characterized by the eastward propagation along the equator. Documentation of seasonal variations of the MJO, particularly details on representation of the meridional propagating mode associated with the Asian summer monsoon variability in these models will be reported separately. If not otherwise specifically defined, hereafter, the winter season refers to the period from November to April. Before we go into an in-depth evaluation of the modeled MJO performances, the models' representation of the winter mean rainfall is first examined to explore possible links between a model's capability in simulating the mean state and the MJO as previously reported [e.g., *Inness and Slingo*, 2003; *Zhang et al.*, 2006; *Kim et al.*, 2009].

Figure 1 illustrates simulated winter mean rainfall patterns along with the observed counterpart based on TRMM (top left). Note that for most analyses present in this study, while model statistics are derived based on 20 year simulations, those for the observations are calculated during the 15 year period of 1998–2012. Sensitivity tests show that mean or variability statistics will not greatly change due to the difference in the data period from 15 to 20 years. The observed winter mean rainfall pattern, including the elongated rain belt along the Intertropical Convergence Zone near 10°N and the South Pacific Convergence Zone (SPCZ) over the western Pacific, as well as rain associated with the convergence zone over the central and eastern equatorial Indian Ocean, is reasonably represented in most of these models. A common positive rainfall bias over the southwest Indian Ocean, as has been widely reported and ascribed to the model excessive response to the local meridional SST gradient [e.g., *Bollasina and Ming*, 2013], is still present in most of these GCM simulations. The mean rainfall over the SPCZ region is greatly overestimated in several GCMs, including BCC-AGCM2.1, ECHAM5-SIT, and UCSD-CAM3.

Figure 2 displays the standard deviation (SD) of 20–100 day band-pass filtered rainfall during boreal winter for both TRMM and GCM simulations, which depicts the amplitude of the intraseasonal variability (ISV) in general. While the ISV amplitude is greatly exaggerated in many GCMs, particularly in BCC-AGCM2.1, CFS2, CWB-GFS, GISS-E2, MRI-AGCM3, and UCSD-CAM3, it is greatly underestimated in many other models, such as CAM5, CAM5-ZM, CanCM4, CNRM-ACM, ECEarth3, and NavGEM1. A close association between the mean rainfall and SD patterns is also noted. Those aforementioned models which exhibit excessive rainfall over the southwest Indian Ocean also largely show stronger rainfall SD over this region. Also, those models that show large mean rainfall biases over the SPCZ also show generally too strong ISV amplitudes. The close association between mean and SD patterns of rainfall in a GCM is further evident by a high correlation of 0.75 between skill for the mean versus SD patterns across the 27 model simulations (not shown). (A correlation coefficient of 0.32 is significant at the 95% level based on a one-tailed Student's *t* test if the 27 individual GCM simulations are independently treated.) Skill in the mean (SD) pattern for a particular model is derived by the pattern correlation between the simulated and observed mean (SD) pattern over the Indo-Pacific domain (60°E–180°; 15°S–15°N).

In the following, two approaches are employed based on rainfall fields to objectively quantify how the observed eastward propagation of the MJO is represented in each model. The first approach is based on a lag-regression method. Before calculation of the regression patterns, daily rainfall during multiyear periods from both TRMM and GCM simulations is subject to removal of the climatological annual cycle (annual mean plus three leading harmonics), and then a 20–100 day band-pass filtering. Spatial distributions of

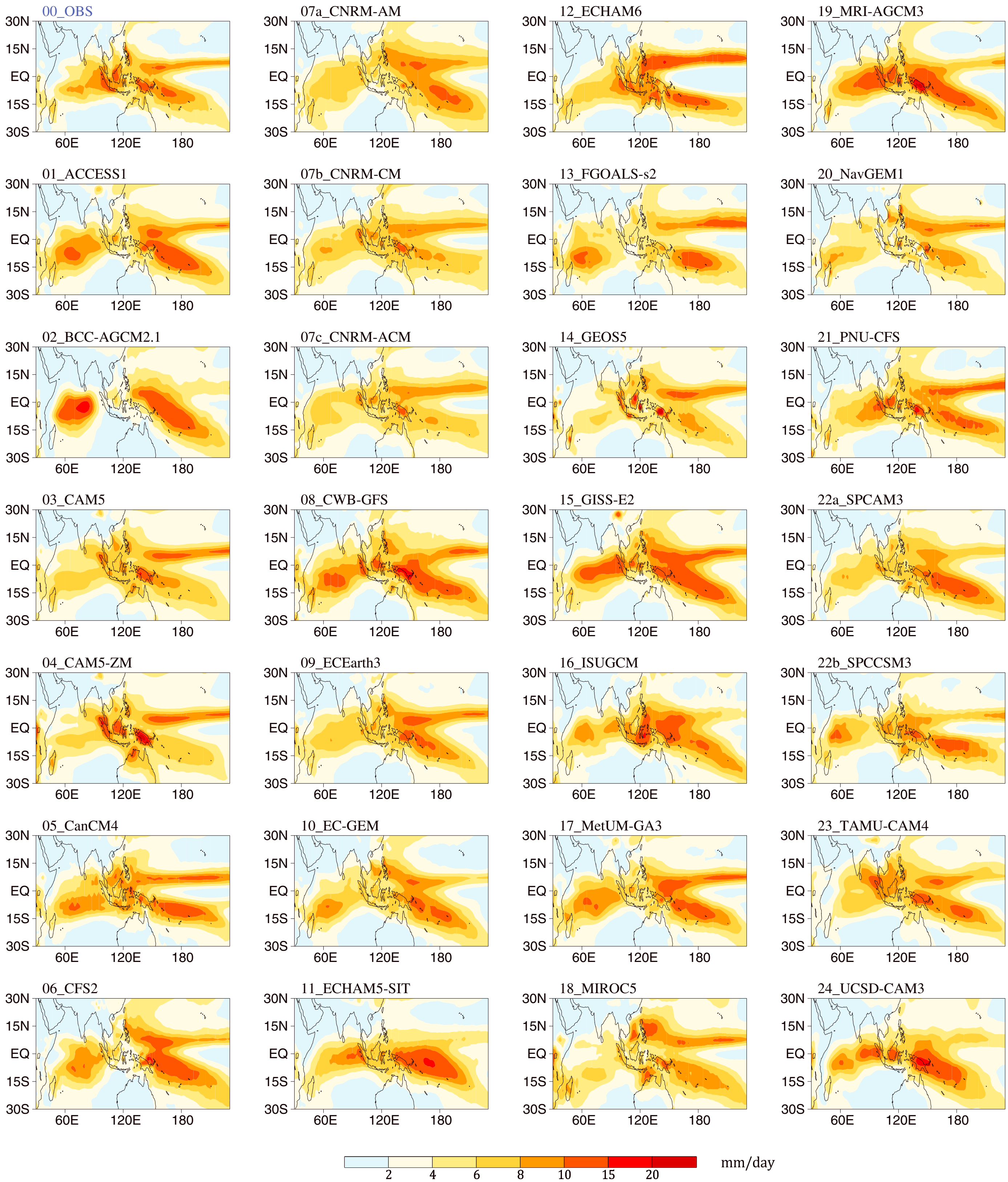

Figure 1. Winter (November–April) mean rainfall based on TRMM observations (1998–2012) and multimodel simulations (20 years).

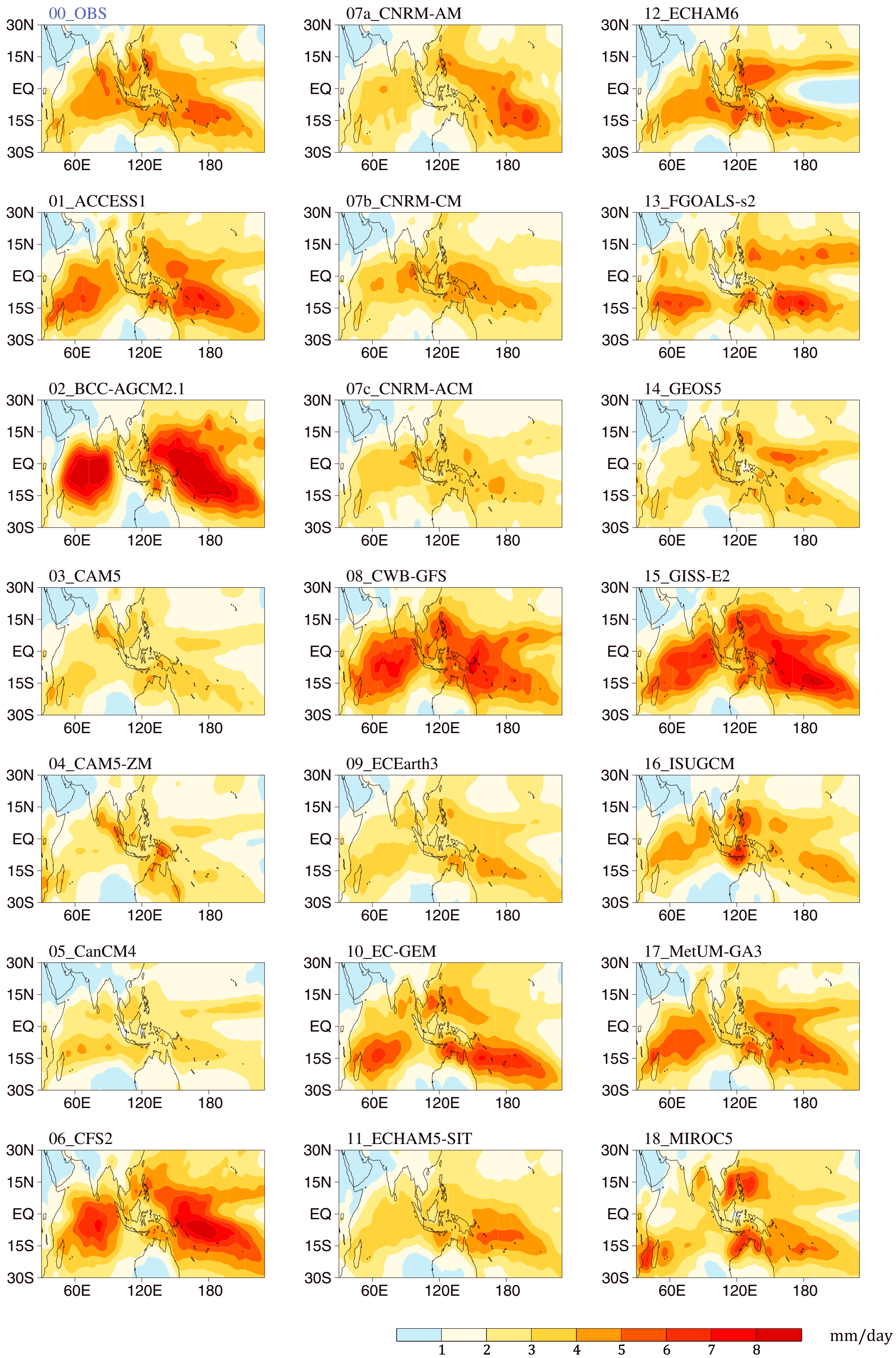

Figure 2. Standard deviation of daily 20–100 day band-pass-filtered rainfall anomalies during boreal winter (November–April) based on observations and model simulations (unit: mm d^{-1}).

regression coefficients based on filtered rainfall are calculated against rainfall anomalies averaged over an Indian Ocean (75–85°E; 5°S–5°N) and a western Pacific (130–150°E; 5°S–5°N) box, respectively, at time lags from day −20 to day 20 with an interval of 1 day. Note that only rainfall data during winter season were used for the lag-regression calculation, and amplitudes in regressed rainfall patterns were determined corresponding to one SD of band-pass-filtered rainfall over these two regions.

Figure 3 presents Hovmöller diagrams (longitude versus time in lag days) of rainfall anomalies along the equator based on the lag regression for both TRMM and GCM simulations against the Indian Ocean base point. The systematic eastward propagation associated with the MJO, starting from the Indian Ocean and dissipating near the dateline at a phase speed of $5° d^{-1}$ (denoted by the slope of the dashed line), is clearly evident in TRMM observations (Figure 3, top left). It is also readily seen from Figure 3 that it still remains challenging for the latest generation of GCMs to capture this eastward propagating MJO mode, as recently reported by analyzing the Coupled Model Intercomparison Project Phase 5 (CMIP5) GCMs [*Hung et al.*, 2013]. Most models participating in this project simulate a stationary or even westward propagating ISV mode over the Indian Ocean. The observed eastward propagating rainfall signals are only reasonably simulated in a limited number of GCMs, including CNRM-CM, ECHAM5-SIT, GISS-E2, MRI-AGCM3, PNU-CFS, SPCCSM3, and TAMU-CAM4. Weaker eastward propagating signals can also be seen in ECHAM6 and SPCAM3, noted by a jump of convection over the Maritime Continent. Moreover, a slower than observed eastward propagation speed is evident in ECHAM5-SIT, MRI-AGCM3, and PNU-CFS. As previously mentioned and reported in *Lappen and Schumacher* [2012], by empirically incorporating the observed heating structure into the CAM4 model, the eastward propagation of the MJO is realistically captured in the TAMU-CAM4. Additionally, associated with enhanced convection over the Indian Ocean at day 0, suppressed convection anomalies are also evident over the western Pacific in most of these several models that capture more realistic eastward propagation, in agreement with findings by *Kim et al.* [2014a] that suppressed convection over the western Pacific could contribute to the eastward propagation of the MJO over the Indian Ocean.

Particularly noteworthy is that while the eastward propagation is poorly captured in the atmospheric-only version of the CNRM GCM (CNRM-AM), it is significantly improved in the coupled version of this model (CNRM-CM). As shown in Figure 3, the CNRM-CM is among one of the top models in capturing the eastward propagation of the MJO. The significant improvement in simulating the MJO by including the coupling strongly suggests the crucial role of the air-sea interaction for the MJO based on this model. The additional run of CNRM-ACM, which is an AGCM integration but forced by the monthly SST and sea ice generated from CNRM-CM, still produces weak eastward propagation. This result suggests that improvement of the MJO in the CNRM-CM run is achieved largely through the interactive processes at the atmosphere and ocean interface, rather than an indirect influence through change in the mean state due to inclusion of the air-sea coupling. Details on the key processes for the improvement of MJO simulations by the air-sea interaction in CNRM-CM are still under investigation, which are expected to provide critical insight into key processes for the MJO.

Similar Hovmöller diagrams of rainfall anomalies as in Figure 3 but based on lag regression against the western Pacific base point are illustrated in Figure 4. In general, most of the models that capture relatively strong eastward propagation over the Indian Ocean as shown in Figure 3 also reasonably well capture the eastward propagation over the western Pacific. While the eastward propagation is well captured over the Indian Ocean in MRI-AGCM3 and SPCCSM3, the propagation across the Maritime Continent is not well resolved in these two models (Figure 4), which may suggest that many ISV events over the western Pacific in these two models tend to be locally initiated, rather than associated with the eastward propagation signals from the Indian Ocean as in the observations. Note that significant improvement in simulating the eastward propagation by including air-sea coupling is again clearly evident in simulations based on the CNRM model, also slightly more realistic eastward propagation is evident in SPCAM3 than that in SPCCSM3.

In order to objectively quantify model skill in capturing the eastward propagation associated with the MJO, pattern correlations are calculated on a time-longitude domain of 60°E–180°and day −20 to day 20 between simulated rainfall evolution patterns and the observed counterpart as shown in Figures 3 and 4. Then the two pattern correlation scores for each model, one from the Indian Ocean and another from western

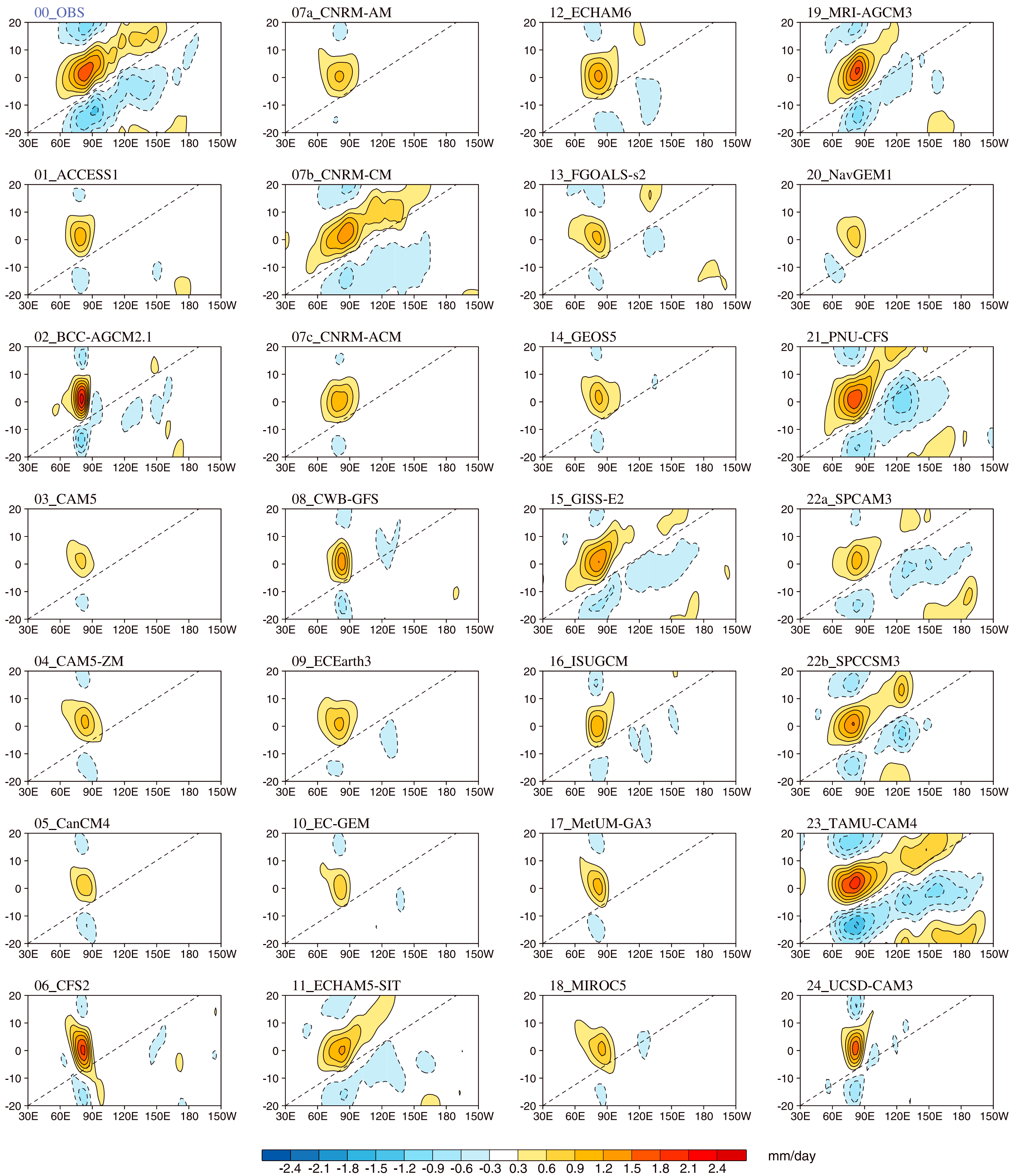

Figure 3. Longitude-time evolution of rainfall anomalies by lag regression of 20–100 day band-pass-filtered anomalous rainfall against itself averaged over the equatorial eastern Indian Ocean (75–85°E; 5°S–5°N). Rainfall anomalies are averaged over 10°S–10°N. Dashed lines in each panel denote the 5 m s^{-1} eastward propagation phase speed.

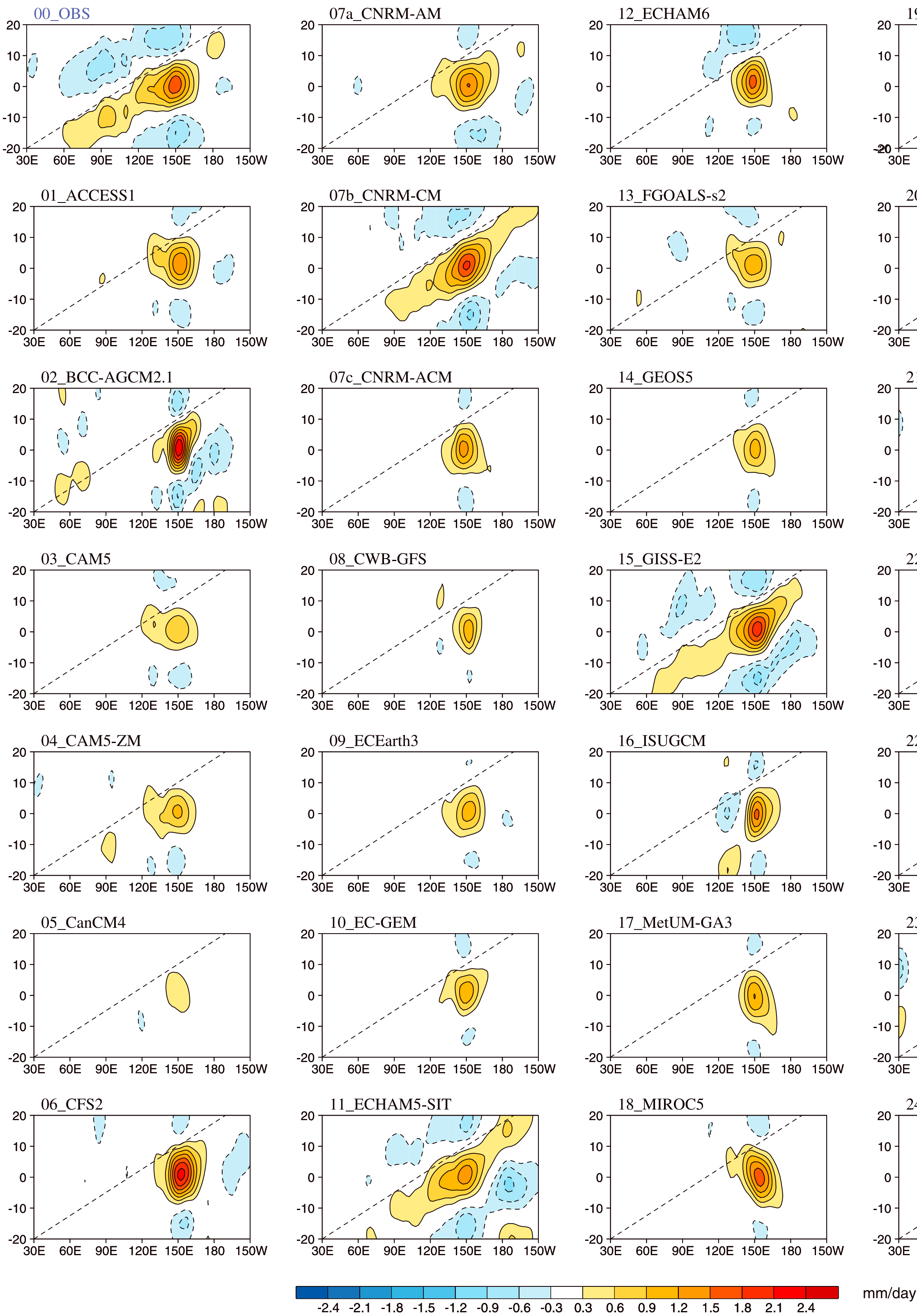

Figure 4. Same as in Figure 3 but by lag regression against rainfall over a western Pacific box (130–150°E; 5°S–5°N).

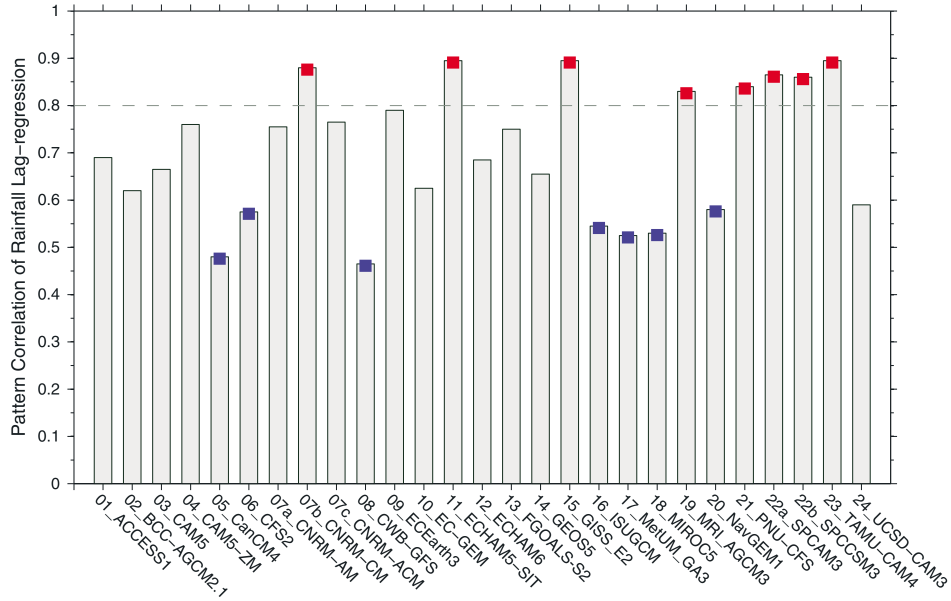

Figure 5. MJO skill scores in GCMs based on pattern correlations of lag-regressed rainfall anomalies on a time-longitude domain (60°E–180; day −20 to day 20) to the observations based on TRMM as shown in Figures 3 and 4. Red and blue squares denote GCMs simulating strong and weak eastward propagation of the MJO. See text for more details in defining the pattern correlation scores and good and poor MJO models.

Pacific-based regression pattern, are averaged to obtain the final skill score in representing the eastward propagation, which is displayed in Figure 5. Among the 27 total simulations, eight models (denoted by red squares), including CNRM-CM, ECHAM5-SIT, GISS-E2, MRI-AGCM3, PNU-CFS, SPCAM3, SPCCSM3, and TAMU-CAM4, exhibit superior skill in simulating the eastward propagation with pattern correlations exceeding 0.8. We then identified these eight GCMs as good MJO models and seven GCMs with the lowest pattern correlation skill (blue squares in Figure 5) as poor MJO models, roughly representing the top 25% and bottom 25% models. The reason that eight GCMs are selected for the good group while seven for the poor one is partially due to the consideration that the MJO skill in the two superparameterized runs (SPCCSM3 and SPCAM3) is very similar; also, many diabatic fields including temperature and moisture tendency terms were not archived from both of these two superparameterized runs. Differences in vertical structure of the MJO between the good and poor MJO model groups will be characterized based on composite analyses in section 5.

Another widely used approach to quantify the model MJO skill is based on the space-time power spectral analysis of rainfall or other convection related variables over an equatorial belt [*Takayabu*, 1994; *Wheeler and Kiladis*, 1999; *Kim et al*., 2009]. The ratio of spectral power for the eastward to westward propagation component (E/W ratio hereafter) on MJO time and space scales has been shown to be a useful indicator to measure the eastward propagation associated with the MJO [*Kim et al*., 2009]. In previous studies, in order to calculate the E/W ratio, the space-time power spectrum analysis (hereafter W-K analysis after the approach by *Wheeler and Kiladis* [1999]) was applied to the global tropical region. In this study, however, we confined the W-K analysis of rainfall from both TRMM and GCM simulations to the Indo-Pacific region from 60°E to the dateline along an equatorial belt. The rainfall data beyond this longitude band were linearly reduced to zero with a transition zone of 20° longitude on both sides. While the MJO skill in these models derived by the E/W ratio based on a global or regional W-K analysis is largely consistent with a correlation of 0.92, one advantage of employing this regional W-K analysis is to provide a more coherent link between the activity of the MJO and CCEWs over the Indo-Pacific in a GCM. Based on a global W-K analysis, the MJO activity could be disconnected from activity of CCEWs. For example, while the maximum MJO variances appear over the Indo-Pacific sector, maximum variances in a global W-K plot for the equatorial Kelvin waves could reflect an activity center over the Atlantic and Africa [e.g., *Kiladis et al*., 2009; *Guo et al*., 2014].

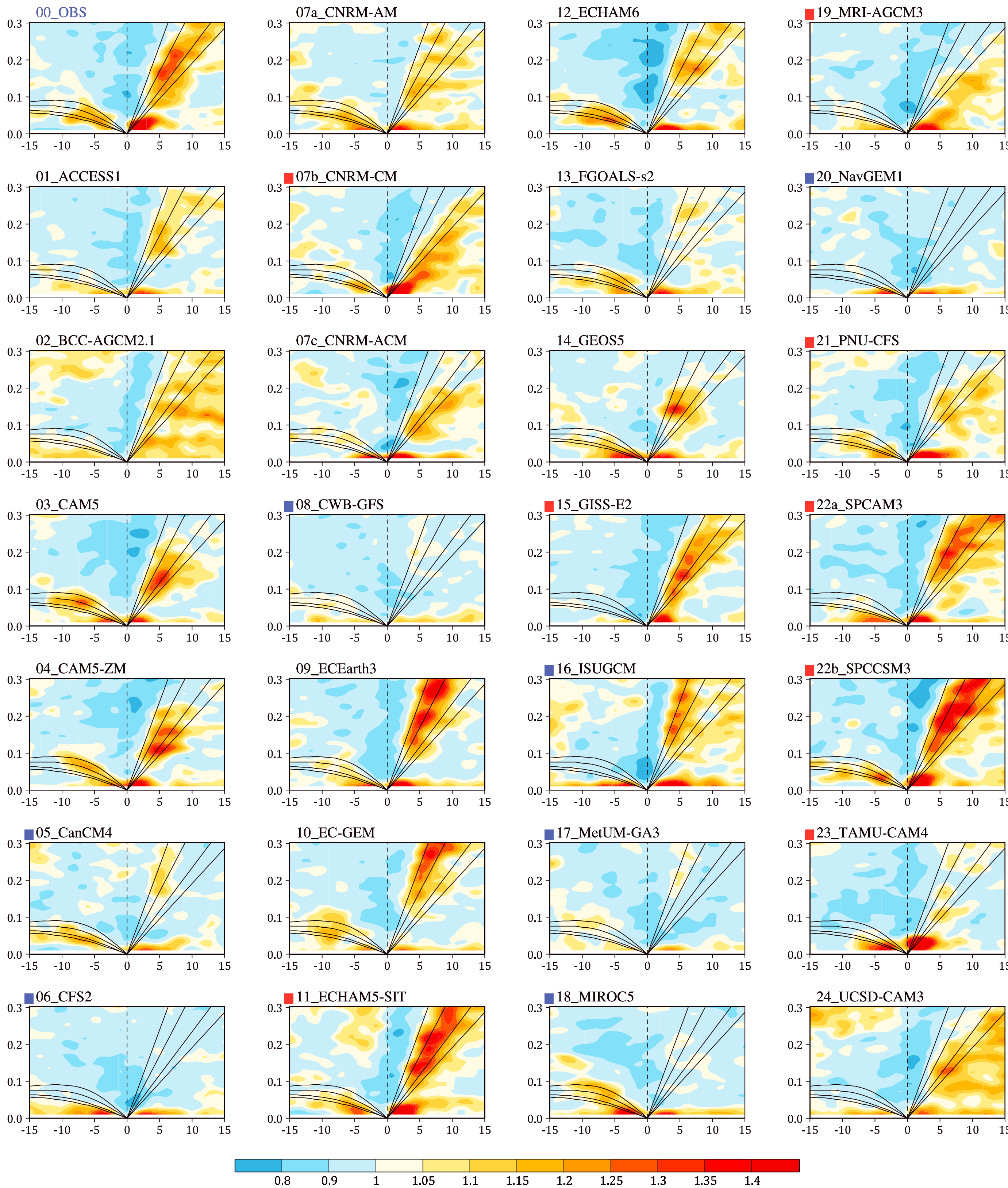

Figure 6. Wave number-frequency power spectra of the symmetric component of equatorial rainfall over the Eastern Hemisphere (60°E–180°), plotted as the ratio between raw rainfall power and the power in a smoothed red noise background spectrum averaged from 15°S to 15°N. Superimposed are the dispersion curves of the equatorial waves for the four equivalent depths of 9, 12, 25, and 50 m. Red and blue squares denote good and poor MJO GCMs identified in Figure 5.

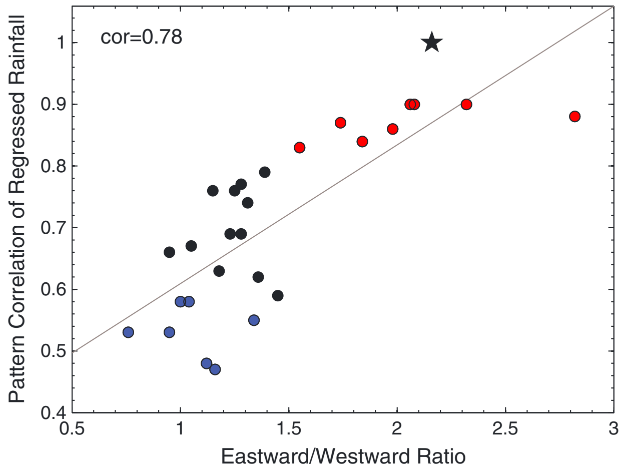

Figure 7. Scatterplot between two measures of MJO skill scores in multimodel simulations, i.e., based on pattern correlation of rainfall Hovmöller diagram (*y* axis) and E/W ratio (*x* axis). Red and blue dots represent GCMs with good and poor MJO as defined in Figure 5, and the star mark represents the observations. The line denotes linear fit by least squares means. The correlation coefficient is also displayed.

Figure 6 displays wave number-frequency spectral variances, normalized by the background spectra following *Wheeler and Kiladis* [1999], for the symmetric component of TRMM and simulated rainfall over the Indo-Pacific region between 15°S and 15°N. In accord with many previous studies, in the observations (Figure 6, top left), variances corresponding to the MJO, equatorial Kelvin (EK), and Rossby (ER) waves stand out from the background spectra. The eight good MJO models (denoted by red squares), identified by the rainfall Hovmöller diagrams, generally exhibit strong variance maxima near the observed MJO wave number-frequency domain, while other models either display very weak spectral variances at MJO scales or variance centers shifted to lower frequency, a typical model deficiency as described in *Lin et al*. [2006]. Also note that the observed spectral variances in both the MJO and EK waves are realistically captured in several good MJO models, including ECHAM5-SIT, GISS-E2, SPCAM3, and SPCCSM3. The EK waves are rather weak in TAMU-CAM4 and exhibit much slower propagation speed in CNRM-CM and MRI-AGCM3. Particularly noteworthy is that variances of the EK waves are generally weak in the seven previously defined poor MJO models (labeled by blue squares). A more detailed analysis on the relationship between the CCEWs and the MJO based on these GCM simulations was reported by *Guo et al*. [2015], which indicates that high-frequency CCEWs may play a role for realistic simulations of the MJO in a GCM. The improvement of MJO variances by the air-sea interaction in the CNRM-CM model is again clearly evident in Figure 6. It is also of interest that the phase speed of the EK waves tends to be slowed down in CNRM-CM and CNRM-ACM compared to that in CNRM-AM, suggesting possible impacts by changes in both the SST distribution and associated circulation on EK wave activity.

The E/W ratio is then calculated based on the W-K diagrams in Figure 6 on a space-frequency domain of zonal wave numbers 1–3 and periods of 30–60 days. The measures of the MJO eastward propagation based on the E/W ratio for TRMM observations and GCM simulations are displayed in Figure 7 along with the skill scores previously derived by the pattern correlation of rainfall Hovmöller diagram. A highly significant correlation of about 0.8 is found between these two measures of MJO skill. The previously defined eight stronger MJO models (denoted by red dots in Figure 7) also show larger E/W ratios in general. This lends us further confidence to use these objectively defined MJO skill measurements for diagnoses of process-oriented metrics as described in the following, to understand key processes for good MJO simulations in GCMs.

Before we go into detailed process-oriented diagnoses of plausible key processes for realistic MJO simulations in next section, we first examine how model MJO performance is related to its skill in simulating the winter mean rainfall climate as shown in Figures 1 and 2. Table 2 illustrates correlation coefficients between model MJO skill score as represented by both the pattern correlation of rainfall Hovmöller diagram and the E/W ratio, and the model winter mean rainfall pattern correlation skill, mean rainfall amplitude, 20–100 day rainfall SD pattern correlation skill, and 20–100 day rainfall SD amplitude over the Indo-Pacific (60°E–180;15°S–15°N). The result suggests that there is no significant correlation in

Table 2. Correlations Between Model Skill for Winter Rainfall Climate Over the Indo-Pacific Region (60°E–180; 15°S–15°N) and MJO Score

	Mean Rain Pattern	Mean Rain Amplitude	20–100 Day Rain SD Pattern	20–100 Day Rain SD Amplitude
Rainfall E/W ratio	0.31	0.16	0.25	0.01
Rainfall pattern correlation	0.30	0.01	0.26	0.02

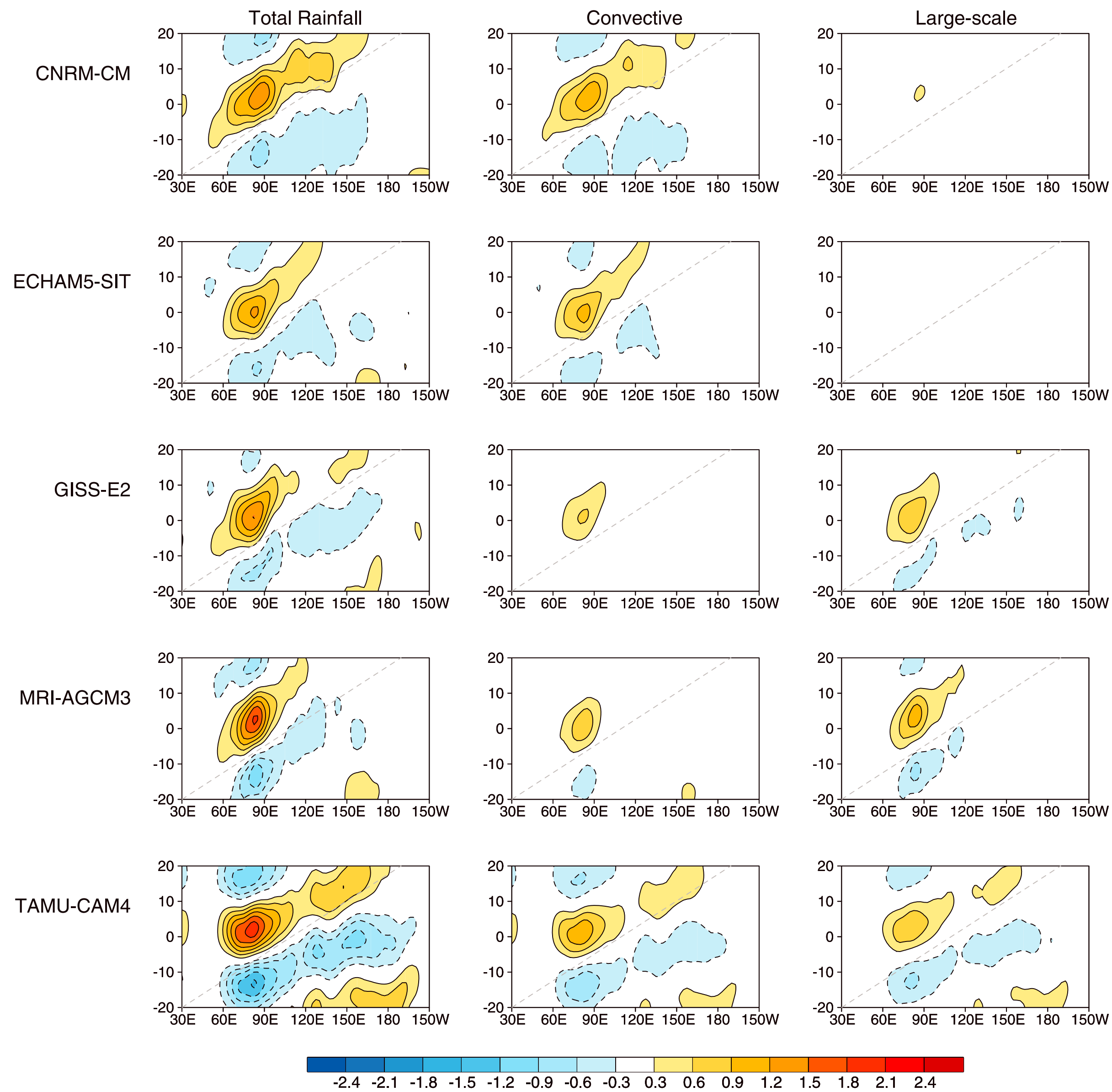

Figure 8. Same as in Figure 3 for longitude-time evolution of (left column) total rainfall anomalies for five good MJO GCMs along with decomposition into (middle column) convective and (right column) large-scale condensation (units: mm d^{-1}).

general between the model MJO fidelity and its skill in simulating the winter mean rainfall climate. In particular, the 20–100 day rainfall SD amplitude over the Indo-Pacific region, which is often used to represent the amplitude of the ISV, exhibits a very weak correlation with the model MJO skill scores.

4. Process-Oriented Metrics for the MJO

4.1. Convective Versus Grid-Scale Precipitation

Previous observational studies suggested that stratiform rainfall plays an important role in producing a top-heavy heating structure [*Houze*, 1982; *Schumacher and Houze*, 2003; *Lin et al.*, 2004]. A top-heavy latent heating profile in climate models, usually associated with large-scale or grid-scale precipitation in analogy to the observed stratiform rain component, is found to be critical for realistic simulations of the MJO [*Fu and Wang*, 2009; *Seo and Wang*, 2010]. A stratiform rain partition ratio of about 40% of total rainfall amount was reported based on TRMM estimates [*Schumacher and Houze*, 2003; *Lin et al.*, 2004; *Jiang et al.*, 2009; *Kim et al.*, 2009]. Although

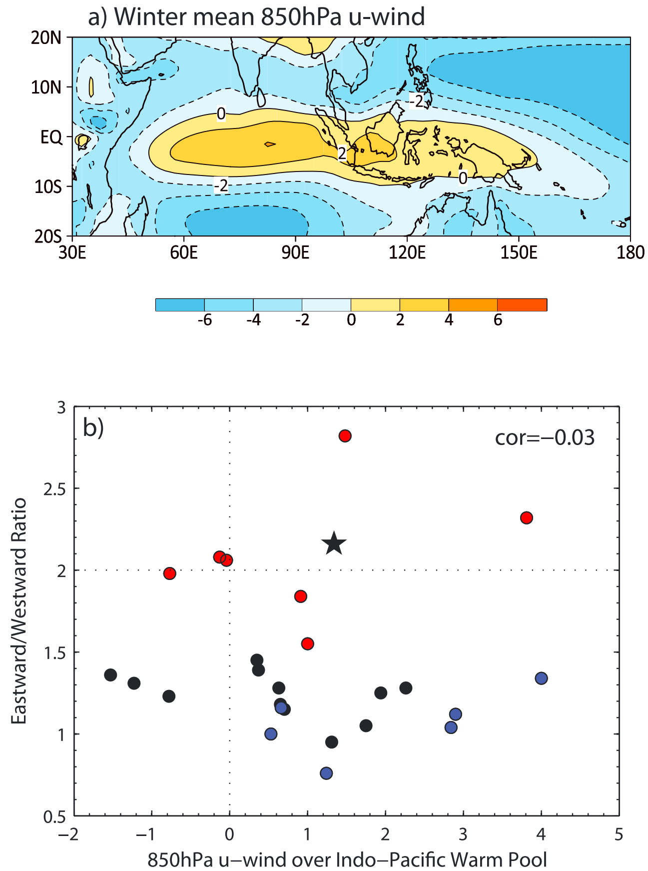

Figure 9. (a) Observed winter mean 850 hPa zonal winds over Indo-Pacific warm pool region based on ERA-Interim reanalysis; (b) Scatterplot between MJO skill score (E/W ratio) and 850 hPa winter mean u-wind averaged over 60–150°E and 5°S–5°N. The units for zonal wind in both Figures 9a and 9b are m s^{-1}.The black star mark represents the observations, and red and blue dots for good and poor MJO model simulations.

caution must be used when directly comparing stratiform rainfall in observations to large-scale rainfall based on GCM simulations due to their different definitions, a much smaller percentage of large-scale rainfall to total rainfall was found in GCM simulations [*Song and Yu*, 2004; *Bechtold et al.*, 2008; *Jiang et al.*, 2009; *Kim et al.*, 2009], which was thought to be one of the factors limiting model capability in simulating the MJO.

In this section, association between large-scale rainfall percentage in winter mean rainfall and a GCM capability in simulating the MJO is explored. To be consistent with several recent diagnostic studies on process-oriented MJO metrics and other research activities coordinated previously by the MJOTF [e.g., *Waliser et al.*, 2009; *Kim et al.*, 2009; *Kim et al.*, 2014b; *Benedict et al.*, 2014], we mainly employ the E/W ratio as the MJO skill measurement for the following analyses. Results are qualitatively similar if the MJO skill scores based on pattern correlations of lag-regressed rainfall evolution (Figure 5) are used for these diagnoses.

Winter mean rainfall was calculated based on the daily averaged rainfall data from November to April. Partition ratios by large-scale rainfall in the mean rainfall in a model are derived on each model grid and then averaged over the Indo-Pacific domain (60°E–180°; 15°S–15°N). The results suggest that there is rather weak correlation (0.11) between the E/W ratio and winter mean large-scale rainfall partition percentage in the model.

The role of convective versus large-scale rainfall for the MJO is further depicted in Figure 8, in which total rain anomalies associated with the MJO were decomposed into convective and large-scale components based on five of the eight strong MJO models (there is no decomposition of the total rainfall in the two superparameterized models; also these data were not archived in PNU-CFS). The Hovmöller diagrams shown in Figure 8 for each model were derived based on the same lag-regression approach as in Figure 3 against rainfall over the Indian Ocean. Comparable contributions from convective and large-scale parts to the total MJO rainfall anomalies are noted in three of these five GCMs (GISS-E2, MRI-AGCM3, and TAMU-CAM4). The amplitude of large-scale rainfall is slightly stronger in GISS-E2 and MRI-AGCM3, while convective rain is slightly stronger in TAMU-CAM4. In contrast, in the other two GCMs, i.e., CNRM-CM and ECHAM5-SIT, convective rainfall dominates over large-scale rain in the total MJO rainfall anomalies. This result agrees with the weak correlations between MJO skill score and large-scale rainfall percentage ratio in total winter mean rainfall, indicating that the role of large-scale rainfall ratio may not be directly related to MJO performance in a GCM.

4.2. Low-Level Mean Zonal Wind

Previous studies have suggested that winter mean low-level zonal wind over the Indo-Pacific, where the prevailing winds are westerly along the equator (Figure 9a), could be critical for the eastward propagation of the MJO convection [e.g., *Inness et al.*, 2003; *Sperber et al.*, 2005; *Zhang et al.*, 2006]. The westerly low-level mean flow is necessary to produce the correct sign of anomalous surface heat fluxes. It is also considered to be an important factor responsible for the eastward propagation of the MJO through eastward advection of anomalous moisture [*Maloney et al*., 2010; *Sobel and Maloney*, 2013]. A significant relationship between winter mean low-level wind and MJO skill, however, was not clearly evident in GCM simulations analyzed in *Kim et al*. [2009]. Analyses by *Benedict et al*. [2013] also illustrated that the quality of simulated zonal mean wind in GCMs tends to be degraded when the MJO simulations are improved. The dilemma in simulating the mean state and MJO was further discussed by *Kim et al*. [2011, 2012].

In this part, we further examine the relationship between seasonal mean low-level zonal wind and MJO skill. A scatterplot of 850 hPa winter mean u-wind averaged over the Indo-Pacific warm pool (60°E–150°E; 5°S–5°N) versus the MJO skill score by the E/W ratio based on the 27 GCM simulations and reanalysis is illustrated in Figure 9b. A rather weak correlation of −0.03 between the mean 850 hPa u-wind and MJO skill is obtained. In contrast to the observed mean westerly zonal wind (denoted by the "star" mark), two strong MJO models are noted with very weak mean zonal winds, while another strong MJO model exhibits easterly wind along the equator. Additional calculation of correlation between model winter mean 850 hPa u-wind pattern skill over 60°E–180 and 15°S–15°N, and the E/W ratio across the 27 model simulations suggests an insignificant coefficient of 0.18. This result agrees with previous results by *Benedict et al*. [2013] and *Kim et al*. [2009] and indicates that factors other than a realistic mean low-level zonal wind could be critical for a realistic simulation of the MJO.

4.3. Vertical Relative Humidity Profiles

Motivated by observational and modeling evidence on the high sensitivity of moist convection to environmental relative humidity (RH) as previously discussed in section 1, there have been several recent studies to examine the saturation fraction or vertical RH profile as a function of rain rate [*Thayer-Calder and Randall*, 2009; *Zhu et al*., 2009; *Kim et al*., 2009; *Del Genio et al*., 2012] and apply these diagnostics to qualitatively distinguish better MJO models from worse ones. Based on a composite analysis of Indian Ocean RH (60–90°E; 10S–10°N), *Kim et al*. [2014b] showed that the difference in lower tropospheric RH (850–700 hPa) between the top 10% and bottom 20% of precipitation events is highly related to model MJO skill based on the CMIP3 and CMIP5 models. A strong relationship between the spread in low-level RH between the top tier and bottom tier of precipitation events and model performance in representing the boreal summer ISV over the eastern Pacific was also noticed based on eight AGCM simulations [*Maloney et al*., 2014], in accord with the contention that models producing stronger convective moisture sensitivity tend to produce a stronger MJO.

Inspired by these previous studies, we further test such a diagnostic in this section. First, composite vertical profiles of RH as a function of rainfall over 60°E–180 and 15°S–15°N during the winter season are derived based on daily RH and rainfall data from observations and each model simulation. Figure 10a portrays the composite RH profile based on the observations, in which the ERA-Interim RH and TRMM rainfall were used. Then, the difference in the 500–850 hPa mass-weighted RH between the top 5% and bottom 10% rainfall events in each model simulation versus the E/W ratio in the corresponding model is shown in the scatterplot of Figure 10b. A statistically significant correlation of 0.45 is obtained between the low-level RH difference in strong and weak rain events and the model MJO score, suggesting that simulation of the MJO could be improved if convective sensitivity to column moisture is increased in the model as proposed in previous studies. Further inspection of Figure 10b, however, suggests that other factors, in addition to the low-level RH difference, could also play a role for a realistic simulation of the MJO in a GCM as most of the participating GCMs, including both good and poor MJO models, show a low-level RH difference between 40% and 50%.

4.4. Convective Versus Radiative Heating

Reduced column radiative cooling (anomalous radiative heating effect) due to cloudiness and increased moisture associated with enhanced MJO convection [*Lin and Mapes*, 2004; *Jiang et al*., 2011; *Ma and Kuang*, 2011] could act as an energy source to destabilize the MJO convection [*Raymond*, 2001; *Sobel and Gildor*, 2003; *Stephens et al*., 2004; *Bony and Emanuel*, 2005]. An enhancement factor of radiative heating (Q_R) for the MJO, as defined by a ratio between the column-integrated Q_R and convective heating [*Lee et al*., 2001; *Lin and Mapes*, 2004], was found to be as large as 40% over the Indian Ocean based on TRMM estimates [*Jiang et al*., 2011]. An enhancement factor of 20% was also noted associated with the two strong MJO events during the recent Dynamics of the Madden-Julian oscillation field campaign [*Johnson et al*., 2014]. The critical role of Q_R for the growth of MJO convection with an enhancement factor of 26% was also illustrated in a cloud-resolving model

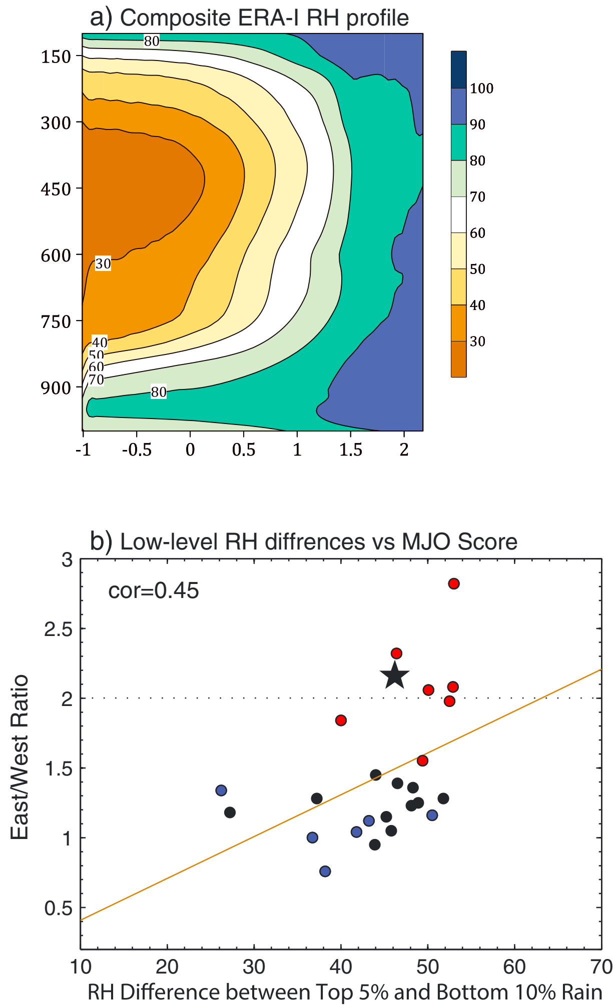

Figure 10. (a) Composite vertical structure of relative humidity based on ERA-Interim as a function of TRMM rain rate over the Indo-Pacific domain (60°E–180°; 15°S–15°N) for November–April during the period of 1998–2012. Note that the rain rate on *x* axis is plotted on a $\log_{10}$ scale; (b) MJO skill score (E/W ratio) versus 500–850 hPa mass-weighted relative humidity difference between the top 5% and bottom 10% of daily rainfall events in observations (star mark) and GCM simulations (dots; red and blue for good and poor MJO GCMs, respectively). The correlation and least squares regression line are also shown.

simulation [*Andersen and Kuang*, 2012]. Particularly interesting is that the MJO tends to be greatly damped when the feedback from Q_R was switched off in that model. Several other modeling studies [e.g., *Slingo and Madden*, 1991; *Lee et al.*, 2001; *Lau et al.*, 2005], however, suggested weakening of the MJO amplitude by enhanced cloud-radiation feedback, possibly due to the bottom-heavy vertical Q_R structure associated with the enhanced MJO convection which tends to suppress deep convection [*Lin et al.*, 2007; *Ma and Kuang*, 2011].

In this section, we explore how the ratio between the Q_R and total latent heating associated with enhanced model convection over the Indian Ocean is related to the MJO skill. The estimate of the enhancement ratio is based on regressed 3-D patterns of Q_R (sum of longwave and shortwave radiation) and latent heating (LH; including convective and stratiform heating, plus shallow and PBL heating if available) against 20–100 day band-pass-filtered rainfall over the Indian Ocean box (75°–85°E; 5°S–5°N) during the winter period of 20 years. The ratio between the 1000–100 hPa vertically integrated Q_R and LH over the Indian Ocean in each model is then calculated based on the regressed patterns. The result indicates a negative but insignificant correlation (−0.19) between the enhancement ratio and MJO skill score by the E/W ratio across multimodel simulations (figure not shown), suggesting that the enhancement ratio by Q_R itself is not a good indicator for the MJO skill in a model. This will be further discussed later.

4.5. Gross Moist Stability

Motivated by recent development in applying the GMS for MJO studies, we further explore how seasonal mean GMS in a GCM is related to its MJO skill. The GMS used in this study was defined following *Raymond et al.* [2009] and *Benedict et al.* [2014], in which specific moist entropy (s) was used as the variable that is conserved under moist adiabatic processes, and moisture convergence as a measure of convective intensity. The vertical (Γ_V) and horizontal (Γ_H) components of GMS are represented as follows:

$$\Gamma_H = -\frac{T_R\left[\vec{v}\cdot\nabla s\right]}{L\left[\nabla\cdot\left(r\vec{v}\right)\right]} \tag{1}$$

$$\Gamma_V = -\frac{T_R\left[\omega(\partial s/\partial p)\right]}{L\left[\nabla\cdot\left(r\vec{v}\right)\right]}, \tag{2}$$

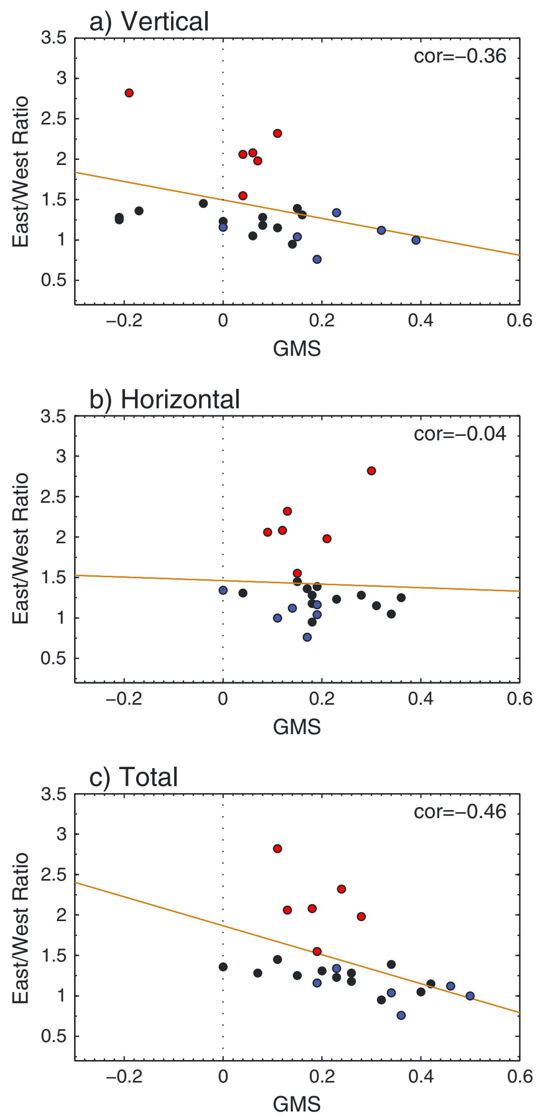

Figure 11. MJO skill score (E/W ratio) versus the (a) vertical component, (b) horizontal component, and (c) total gross moist stability averaged on oceanic grid points over the domain of 60°–150°E and 15°S–15°N. Red and blue dots represent GCMs with good and poor MJO. The correlation and least squares regression line are also shown in each panel.

where the brackets represent a mass-weighted vertical integral from 1000 hPa to 100 hPa, $\vec{v}$ is the horizontal vector winds, T_R is the reference temperature of 273.15 K, ω the vertical pressure velocity, L is the latent heat of vaporization (2.5×10^6 J Kg^{-1}), and r is the water vapor mixing ratio.

Following *Benedict et al.* [2014], before calculating the daily horizontal and vertical components, as well as the total GMS with the above 2.5° × 2.5° daily averaged variables, the numerator and denominator are smoothed with a 7.5° × 7.5° sliding box spatial smoother, and land points are omitted from the calculation. Additionally, to avoid division by zero, daily GMS values over grid points, where the denominator has an absolute value less than 5 W m^{-2}, are set to be missing and are excluded from the calculation for winter mean GMS values. For further details on the computation of GMS, readers are referred to *Benedict et al.* [2014].

Figure 11 illustrates winter mean horizontal, vertical, and total GMS averaged over 60–150°E, 15°S–15°N based on each model simulation versus the model MJO skill represented by the E/W ratio. A statistically significant negative correlation (−0.36) between the model MJO skill and winter mean vertical GMS over the Indo-Pacific is evident (Figure 11a), which is in accord with previous analyses of GMS for the MJO [*Raymond and Fuchs*, 2009; *Raymond et al.*, 2009; *Hannah and Maloney*, 2011; *Benedict et al.*, 2014] and boreal summer ISV over the eastern Pacific [*Maloney et al.*, 2014]. This result tends to support the argument that lower vertical GMS helps to maintain moisture anomalies that support intraseasonal convection. In contrast to previous studies that suggested the horizontal GMS largely compensates the vertical component and exhibits a significant positive correlation to the model MJO/ISV skill, Figure 11b suggests a rather weak correlation between the horizontal GMS and model MJO skill. A stronger negative correlation (−0.46) between the total GMS and MJO skill is discerned in Figure 11c, which also behaves differently than reported in *Maloney et al.* [2014], where total GMS is not significantly correlated to the model ISV skill due to near cancelation of the horizontal and vertical components. While analysis of GMS based on GCMs analyzed in this study tends to support previous studies that a smaller GMS could be conducive for the MJO development, Figure 11c also indicates that the GMS is not able to exclusively explain the MJO skill in some GCMs, for example, a majority of GCMs including both good and poor MJO models exhibit GMS values between 0.1 and 0.3.

Note that based on previous theoretical studies on the MJO mechanism [e.g., *Sobel and Maloney*, 2013], a negative GMS, or effective GMS which includes cloud-radiative feedback, is necessary to destabilize an intraseasonal mode. Whether this unstable intraseasonal mode is able to be organized into an MJO-like system, however, is regulated by other factors that are still not well understood. As shown in Table 2, the

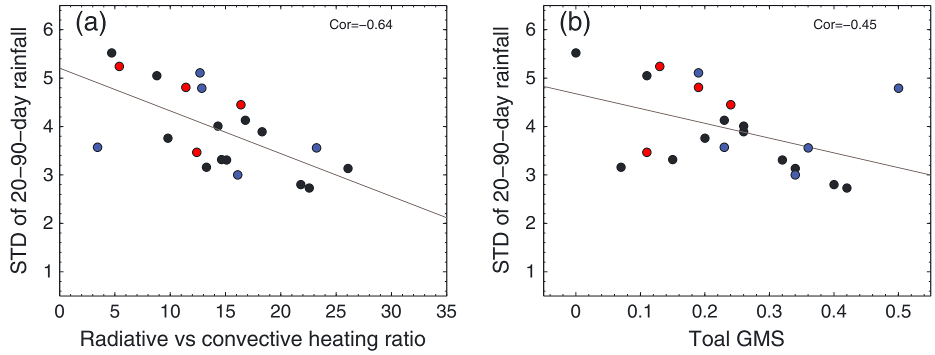

Figure 12. Amplitude of the ISV as denoted by SD of rainfall over the Indo-Pacific warm pool during boreal winter versus the (a) ratio of radiative to latent heating (%); (b) total GMS averaged on oceanic grid points over the domain of 60°–150°E and 15°S–15°N as in Figure 11c. Red and blue dots represent good and poor MJO models. The correlation coefficients and least squares regression lines are also shown.

winter ISV amplitude over the Indo-Pacific region is very weakly correlated to the MJO skill based on these GCM simulations. This notion motivated us to further explore a plausible association between the GMS as well as Q_R versus LH ratio and the ISV amplitude in a model as represented by the SD of 20–100 day filtered rainfall during boreal winter over the Indo-Pacific (60°–150°E; 15°S–15°N). The scatterplots for ISV amplitude versus Q_R ratio and the total GMS are illustrated in Figure 12. Intriguingly, the results suggest that both the Q_R ratio and the total GMS exhibit significant correlations to the ISV amplitude, with high correlations of −0.64 and −0.45, respectively. While a smaller GMS is conducive for stronger ISV, which is consistent with previous discussions, it indicates that a larger Q_R versus LH ratio tends to be associated with weaker ISV amplitude in a model, at odds with the radiative instability theory for the MJO mentioned in section 1. Further investigations are warranted for a better understanding of these results.

5. Vertical Structure of the MJO in GCMs With Good and Poor MJO

In this section, we further explore essential differences in the vertical structure associated with the MJO in good and poor MJO models, which may further provide insight into key processes responsible for realistic simulations of the MJO in climate models. We focus analyses in this part on the MJO over the Indian Ocean.

First, 3-D structure of u-wind (u), temperature (T), vertical p velocity (ω), total atmospheric diabatic heating (Q), and specific humidity (q) associated with intraseasonal convection over the Indian Ocean in each model is derived based on a regression method. Before calculation of the regression, daily 3-D fields of these variables during the 20 year period are subject to removal of the climatological annual cycle (annual mean plus three leading harmonics). Then lag 0 regression patterns of these anomalous 3-D fields are calculated against the 20–100 day band-pass-filtered rainfall averaged over the eastern equatorial Indian Ocean (75–85°E; 5°S–5°N) during the 20 winters. Different from the derivation of lag-regression rainfall patterns in section 3, the amplitudes of 3-D regression patterns here are determined by fixed 3 mm d^{-1} of rainfall across the models, rather than 1 SD of rainfall over the Indian Ocean box applied in section 3. The reason for conducting regression patterns in this way is to focus on the vertical structure of these variables in model simulations rather than their amplitudes. Composite 3-D fields of these above variables can be further calculated for the two groups of GCMs, i.e., good versus poor MJO models as identified in Figure 5. To facilitate a benchmark for model simulations, corresponding 3-D structures of ERA-Interim u, T, ω, Q, and q corresponding to 3 mm d^{-1} of TRMM rainfall are also obtained for the period of 1998–2012 by using a similar regression approach. Note that total diabatic heating based on ERA-Interim was derived by applying a residual budget analysis approach based on the temperature equation [*Yanai et al.*, 1973; *Jiang et al.*, 2009].

Figure 13 illustrates vertical-longitude profiles of u, T, ω, Q, and q along the equator associated with intraseasonal convection over the Indian Ocean for ERA-Interim (top row), as well as good (middle row) and poor (bottom row) MJO models. The observed vertical structure associated with the MJO shown in Figure 13 is consistent with many previous studies [e.g., *Sperber*, 2003; *Kiladis et al.*, 2005; *Jiang et al.*, 2011].

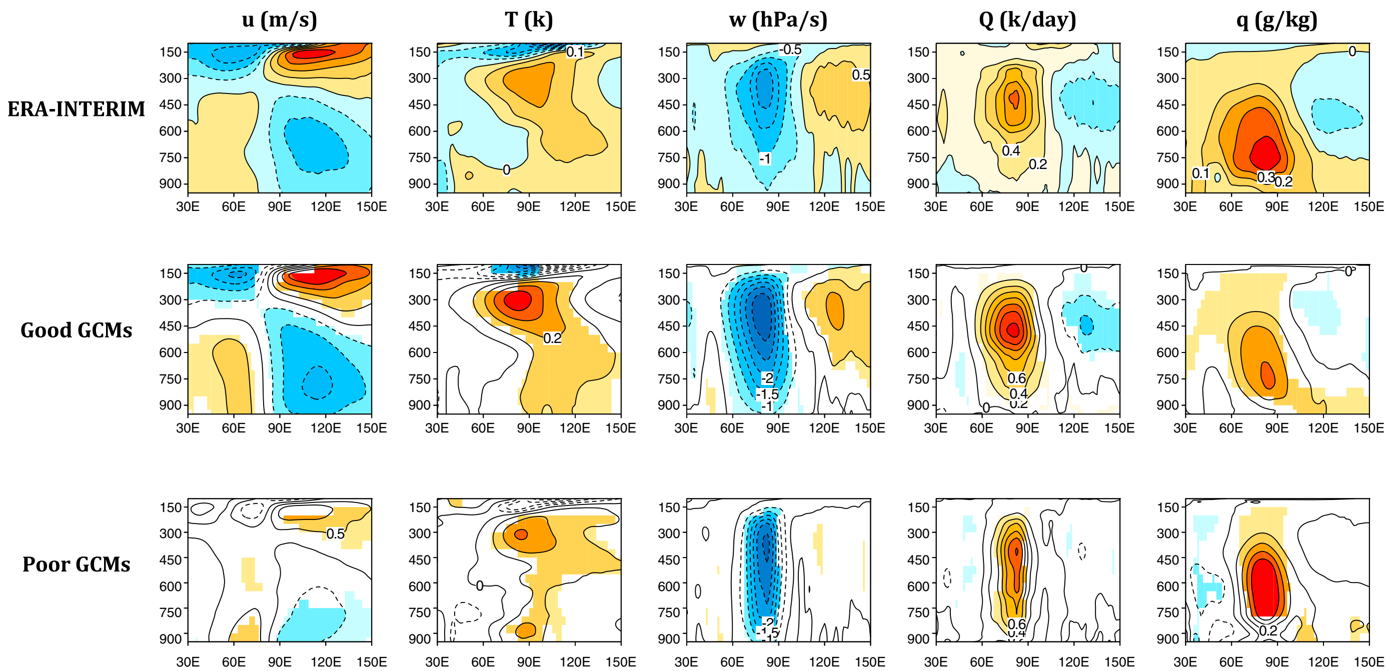

Figure 13. Vertical-longitudinal profiles of zero lag-regressed zonal wind (*u*), temperature (*T*), vertical velocity (*w*), diabatic heating (*Q*), and specific humidity (*q*) onto 20–90 day band-pass-filtered Indian Ocean rainfall (75–85°E; 5°S–5°N) based on (top row) ERA-Interim, (middle row) composites over good and (bottom row) poor MJO GCMs. All variables are averaged over 10°S–10°N. For model composite results, only those significant at 95% level are shown by shaded color.

A baroclinic structure is discerned in anomalous u-wind with low-level westerlies (easterlies) to the west (east) of the convection center and a reversed sign at upper levels. Also evident is a top-heavy structure in positive *T*, upward motion, and diabatic heating structure, as well as an eastward shift of positive moisture, heating, and upward motion in the PBL relative to the convection center, signaling the preconditioning process for the eastward propagation of MJO convection. These prominent features in the observed vertical MJO structure are well represented in good MJO models. In stark contrast, very different vertical structures are noted in the composites for poor MJO models. The baroclinic structure in u-wind, particularly the upper tropospheric circulation, is not well organized in these models. Meanwhile, the second baroclinic mode in *T* with positive anomalies in upper troposphere is also not clearly defined. Previous studies suggested that positive covariance in high-order vertical baroclinic modes between anomalous *T* and ω, and *T* and *Q*, could be critical for growth of MJO convection through generation of EAPE and conversion to eddy kinetic energy [*Fu and Wang*, 2009; *Zhou et al*., 2012]. Also, the westward vertical tilt with height in anomalous ω, *Q*, and *q* fields, which is clearly evident in ERA-Interim and good MJO model simulations, is not as apparent in poor MJO model simulations. Instead, a strictly vertical structure is seen in ω and *Q*. Additionally, a narrower longitudinal extension in upward motion and heating corresponding to the enhanced convection is noted in poor MJO models compared to their counterparts in reanalysis and good model simulations.

Details of how the improved representation in vertical profiles of these above variables is related to MJO performance are further explored in Figure 14. Model skill in simulating the vertical structure associated with the MJO is assessed by conducting pattern correlations of longitude-pressure profiles of *u*, *T*, ω, *Q*, and *q* shown in Figure 13 over a domain of 30°–150°E and 1000–100 hPa between each model simulation and the observations. The results are displayed in scatterplots in Figure 14 on the *x* axis along with corresponding MJO skill score on the *y* axis in Figures 14a–14e, respectively. A scatterplot between averaged skill for vertical structure of these five variables and MJO skill in a model is also plotted in Figure 14f. Good (poor) MJO GCMs are denoted by red (blue) dots in each panel. Note that to be consistent with the approach in defining the good and poor MJO models as in Figure 5, the MJO skill scores based on pattern correlation of rainfall Hovmöller diagrams were also used in this figure. It is clearly evident that model skill in simulating vertical structures associated with the intraseasonal convection in a

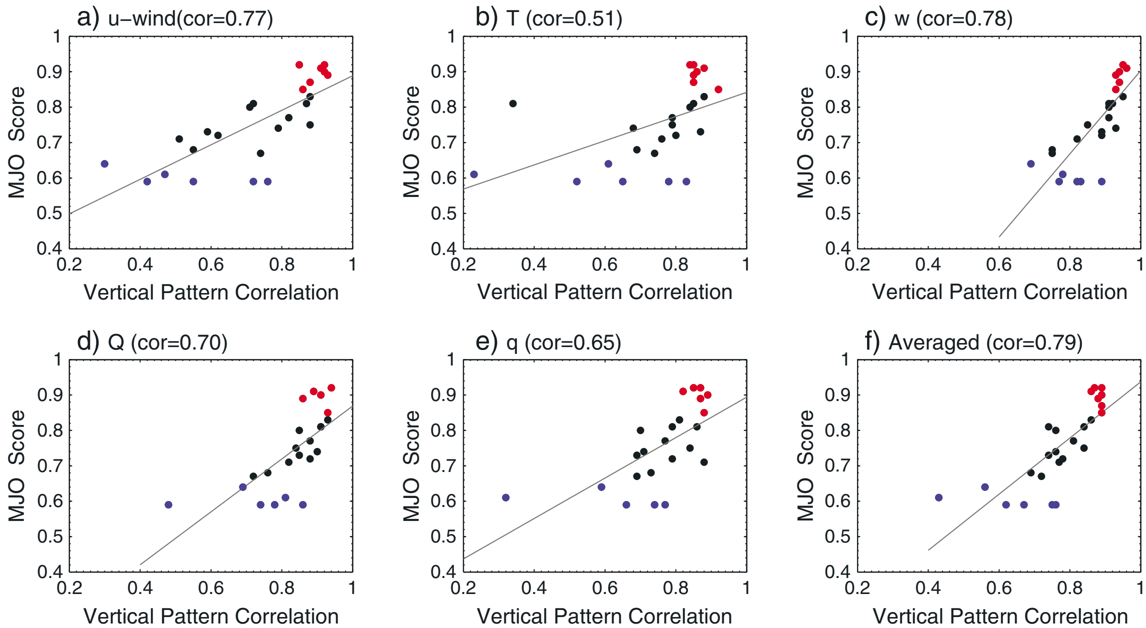

Figure 14. MJO skill score (pattern correlation of rainfall Hovmöller diagram) versus pattern correlation of vertical structures of (a) zonal wind, (b) temperature, (c) vertical velocity, (d) total diabatic heating, (e) specific humidity, and (f) averaged over five variables. Red and blue dots represent good and poor MJO GCMs. Correlations and least squares fit lines are also shown in each panel.

model is highly related to its MJO performance, particularly for u, ω, and Q, with correlation coefficients surpassing 0.7. All the good MJO GCMs exhibit the highest skill in capturing the vertical structure in all these variables. A correlation between the averaged skill over these five variables and MJO skill score is about 0.8, suggesting that a realistic representation of vertical structures in these dynamical and thermodynamical fields is likely essential for a quality representation of the MJO in the model.

One significant deficiency in poor MJO models in capturing the vertical profiles associated with the intraseasonal convection is the lack of vertical tilting structure. As previously discussed, the eastward shift in upward motion, shallow heating, and accumulation of positive moisture anomalies in the PBL to the east of the MJO convection could be critical for the eastward propagation of the MJO. This is also supported by further experiment based on TAMU-CAM4, which confirms that the low-level heating ahead of the MJO convective center is critical for the initial strengthening and eastward migration of the MJO convection in this model [*Lappen and Schumacher*, 2014]. Therefore, these preconditioning processes missing in the poor MJO models could be the essential reasons for their inability to simulate the MJO. Since this preconditioning process is intimately associated with PBL convergence, examination of horizontal circulation and convergence fields will provide further insight into the model deficiencies.

Figure 15 illustrates anomalous rainfall (contours), 925 hPa winds (vectors), and convergence (shaded) derived by regressing onto 3 mm d^{-1} intraseasonal convection over the Indian Ocean for observations, as well as composites for both good and poor MJO models. In the observations (Figure 15a), the low-level convergence associated with enhanced convection is clearly evident. A typical Gill-type anomalous circulation [*Gill*, 1980] is readily discerned with two off-equatorial Rossby wave gyres to the west and equatorial easterlies of the Kelvin wave responses to the east. Local maxima in convergence are discerned over the Maritime Continent near Sumatra and Borneo Islands, in accord with the aforementioned eastward shift of shallow upward motion, heating, and moisture accumulation, again indicating a key preconditioning process for the MJO. The local convergence center to the east of the convection center over the Maritime Continent is well captured in the good MJO models along with realistic Rossby and Kelvin wave responses, although with slightly stronger amplitudes (Figure 15b). In contrast, in poor MJO model simulations (Figure 15c), enhanced rainfall as well as low-level convergence is narrowly confined near the convection center over the Indian Ocean. In association with much weaker Kelvin wave responses, the eastward extension of the convergence zone is not clearly evident. In contrast, strong

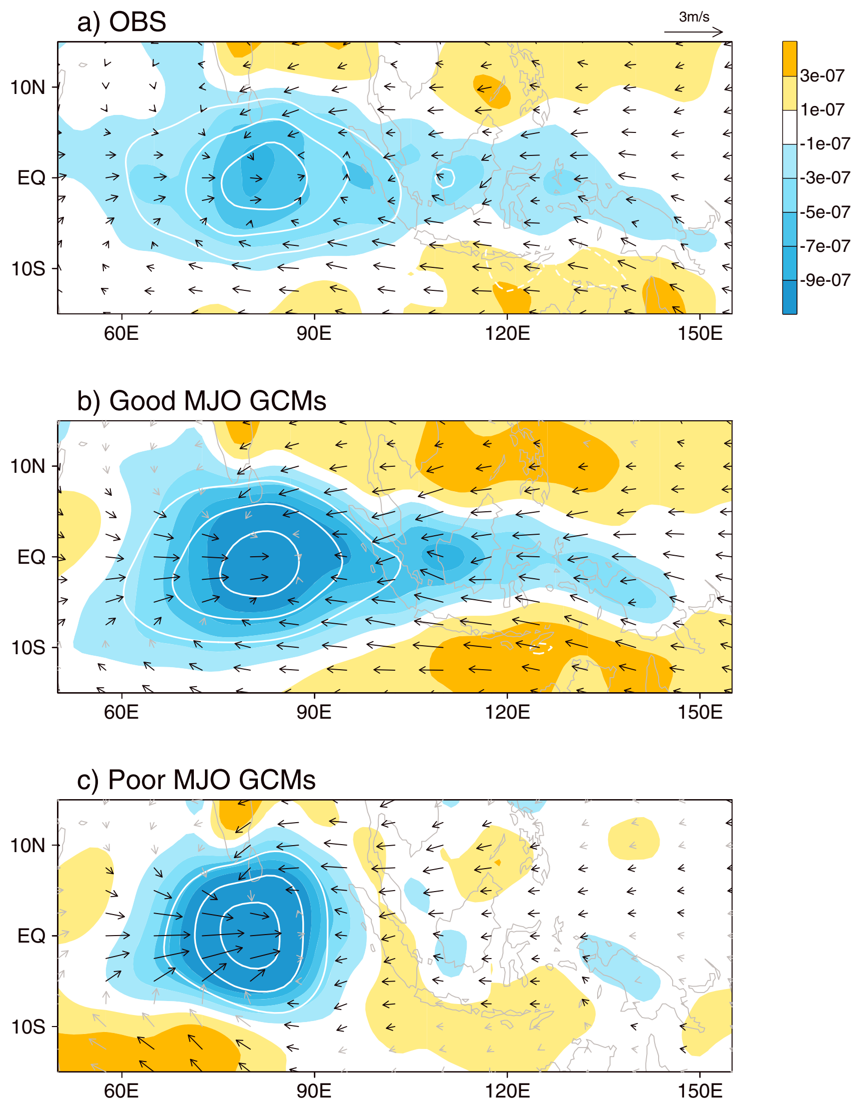

Figure 15. Horizontal patterns of anomalous divergence (shaded; units: s^{-1}; see color bar on top right), rainfall (contour; units: $mm\,d^{-1}$), and winds (vectors; $m\,s^{-1}$; see vector scale on top right) at 925 hPa corresponding to a $3\,mm\,d^{-1}$ rainfall anomaly over the Indian Ocean (75–85°E; 5°S–5°N) based on (a) observations and composites for (b) good and (c) poor MJO models. Only contours of rainfall anomalies at 1, 2, and $3\,mm\,d^{-1}$ are displayed. In Figures 15b and 15c, regions where composite zonal 925 hPa u-wind anomalies are significant at 95% level are denoted by black vectors.

Rossby wave responses to the west of convection are discerned in the poor MJO models. While the physics ascribed to the differences in Rossby and Kelvin wave responses to an intraseasonal convection in good and poor GCMs warrant further investigation, these results suggest that the weakly organized Kelvin wave to the east of convection, and thus the lack of PBL convergence through the Frictional CISK mechanism in the poor MJO models, could be the critical model deficiency leading to low-quality MJO simulations in these models.

6. Summary and Discussions

While the MJO exerts widespread influences on global weather and climate systems, a lack of understanding of the key processes of the MJO greatly limits our capability to simulate the MJO and the skill of extended-range climate predictions. Given the central role of diabatic heating for the MJO physics and motivated by recent progress in characterizing MJO structures based on the observations, a global model evaluation project on the vertical structure and physical processes of the MJO has been jointly coordinated by the former YOTC (now WGNE) MJO Task Force (MJOTF) and GEWEX Atmospheric System Study (GASS) program. In this study, some details of this project were introduced, and results were reported with a particular emphasis on the climate simulation component of this project.

A series of diagnostic methods have been applied to objectively evaluate MJO skill in multimodel simulations and to explore essential model physics responsible for realistic MJO representation. These include the following: (1) longitude-time lag regressions of precipitation relative to rainfall averaged over Indian Ocean and Western Pacific boxes; (2) the ratio of spectral power for the eastward to westward component (E/W ratio) based on wave number-frequency analysis of rainfall fields; (3) vertical structure of u, T, w, Q, and q based on regressions onto rainfall over an Indian Ocean or western Pacific box; (4) regressed patterns of anomalous rainfall and low-level horizontal divergence and winds; (5) composite vertical structure of relative humidity (RH) as a function of rain rate and the low-level RH difference for top and bottom rainfall events; (6) total summer mean gross moist stability (GMS) as well as its contributions from horizontal and vertical components; and (7) the ratio of radiative heating (Q_R) to latent heating as an enhancement factor of Q_R for the MJO.

Analyses show that the MJO continues to represent a great challenge for these latest generation GCMs. The systematic eastward propagation of the MJO is only reasonably well simulated in about eight out of the total 27 GCM simulations. A majority of GCMs only capture a stationary or even westward propagation mode associated with the intraseasonal rainfall variability. Two groups of GCMs, namely, GCMs with good and poor MJO, were then identified based on MJO skill scores, defined by pattern correlations of simulated rainfall Hovmöller diagrams against observations. Composite analyses of longitude-height profiles of several variables along the equator reveal significant differences in vertical structure associated with the MJO between these two GCM groups. In GCMs with good MJO, the observed vertical tilting structure in vertical velocity, diabatic heating, and specific humidity anomalous fields corresponding to enhanced intraseasonal convection is very well captured. In contrast, these observed vertical structures are not simulated in poor MJO models. In particular, no obvious vertical tilt is evident in anomalous vertical velocity, heating, and moisture fields, suggesting that key physics is missing for the MJO preconditioning process in the poor MJO models, albeit it is still arguable whether the vertical tilting structure leads to realistic MJO simulations in good MJO models.

Moreover, composite results in this study suggest large deficiencies in the vertical profiles of u-winds in the poor MJO models (Figure 13). The baroclinic structure in the vertical u-wind as clearly evident in the observations is not well captured in poor MJO models, particularly the divergent flow in the upper troposphere. It would be interesting to further explore in the future work whether the misrepresentation of the cumulus momentum transport effect, which has been shown to be important for the MJO based on previous observational and modeling studies [*Tung and Yanai*, 2002; *Majda and Stechmann*, 2009; *Deng and Wu*, 2010; *Deng and Wu*, 2011; *Miyakawa et al.*, 2012; *Zhou et al.*, 2012; *Oh et al.*, 2015], is responsible for model deficiencies in simulating the vertical structures of anomalous winds in poor MJO models.

Further examination of lower tropospheric circulation associated with intraseasonal convection illustrates that much weaker Kelvin wave, but stronger Rossby wave, responses are discerned in the poor MJO models compared to both the good MJO models as well as the observations. The weak anomalous Kelvin wave responses in the poor MJO models can lead to the absence of PBL convergence to the east of convection center through the Frictional CISK mechanism [e.g., *Wang and Li*, 1994; *Maloney and Hartmann*, 1998], which is considered a critical process for the eastward propagation of the MJO. Further investigations are needed to fully understand the differences in low-level planetary-scale wave responses to a fixed intraseasonal convection anomaly between the good and poor MJO GCMs, which could provide useful information on deficiencies in these poor MJO models. It is also of interest to note that activity of synoptic-scale Kelvin waves is also rather damped in most of the poor MJO GCMs as previously discussed (see Figure 6), which will be reported in more detail in a separate manuscript [*Guo et al.*, 2015]. Possible links between the planetary- and synoptic-scale Kelvin wave activities also warrant further investigation. There could be scale interactions involved in this link between the planetary- and synoptic-scale Kelvin waves. Another possibility is that the activity of these two different scales of Kelvin waves could be modulated by the same mean state, e.g., through the large-scale vertical wind shear [*Zhang and Geller*, 1994; *Wang and Xie*, 1996; *Han and Khouider*, 2010; *Khouider et al.*, 2012; *Guo et al.*, 2014]. Also note that lack of the essential preconditioning processes in the poor MJO GCMs might be also related to their deficiencies in depicting a previous cycle of suppressed convection to the east of the present active convection, which was found to play a role for the initiation or eastward propagation of the MJO [*Sperber*, 2003; *Matthews*, 2008; *Kim et al*., 2014a].

Five process-oriented diagnostics for the MJO were further performed to discriminate key processes responsible for realistic simulations of the MJO in participating GCMs. Three diagnostic metrics, including the large-scale rainfall partition, mean low-level zonal wind, and the Q_R versus LH ratio, were found to not be significantly correlated to the MJO skill represented by the eastward versus westward spectral variance ratio across multimodel simulations. For example, based on simulations from five good MJO GCMs, while the amplitudes in convective rainfall are comparable to those of the large-scale rainfall in three GCMs, the total rainfall associated with the MJO is dominated by convective rain in the other two models. Consistent with previous diagnoses [*Kim et al*., 2014b; *Maloney et al*., 2014], our results suggest that the low-level RH difference between the top 5% and the bottom 10% of precipitation events exhibits statistically significant correlations to MJO performance. These results suggest that the model MJO can be improved with increased convection sensitivity to environmental moisture, in accord with many previous modeling studies. Moreover, a statistically significant negative correlation between the winter mean GMS and MJO skill, as suggested by *Raymond et al*. [2009] and supported by recent diagnostics [*Benedict et al*., 2014; *Maloney et al*., 2014], is further confirmed by analyses in this study, indicating that models in which convection and associated divergent circulations are less efficient at discharging moisture from the column are better able to sustain a strong MJO. However, both the RH difference between the high- and low-rainfall events and the seasonal mean GMS are not able to exclusively explain the model MJO skill.

It is worth noting that air-sea interaction may play a critical role for a realistic simulation of the MJO, as illustrated by experiments based on the CNRM model. While it is very weakly captured in the CNRM AGCM with specified observed monthly SST and sea ice, the eastward propagation of the MJO is rather realistically represented in a coupled version of this model. A third experiment, based on an AGCM run of the CNRM model but forced by the SST and sea ice from the coupled experiment, also exhibits a weak model MJO, further supporting the role of air-sea interaction for the MJO. Detailed physical processes leading to the significant improvement of MJO simulations due to air-sea interaction in the CNRM GCM need to be further explored. Many modeling studies also suggest great improvement of MJO simulation by including the air-sea interaction in the model [e.g., *Sperber et al*., 2005; *Klingaman and Woolnough*, 2014; *Tseng et al*., 2014]. However, controversial results on the role of air-sea interaction on the MJO simulations have been indicated by previous studies, as also suggested by relatively similar MJO skill based on the two superparameterized runs, i.e., SPCAM3 and SPCCSM3, in this study. By analyzing the moist budget based on three different CAM models, *DeMott et al*. [2014] concluded that different model physics involved with the changes in surface fluxes by ocean coupling will strongly influence the moistening processes in these models, which can thus lead to model-dependent responses to air-sea coupling in MJO simulations. A comprehensive review on the role of air-sea interaction on the MJO was recently given by C. A. DeMott, et al., (Atmosphere-ocean coupled processes in the Madden-Julian oscillation, submitted to *Reviews of Geophysics*, 2015).

It is also interesting to note that while the Q_R versus LH ratio is not significantly correlated to MJO skill in a model, a highly significant correlation is found between the Q_R ratio and the ISV amplitude. When the Q_R versus LH ratio (i.e., the cloud-radiation feedback) increases, the ISV amplitude tends to be decreased, which is at odds with the radiative instability theory proposed in several previous studies. While the degraded MJO simulations with the enhancement of cloud-radiative feedback were also reported in several modeling studies, the underlying physics needs to be further explored.

One of the objectives of this project is to explore the possible link between model skill in simulating the intrinsic MJO mode and its practical predictive skill for the MJO in a forecast mode. While this will be discussed in more detail in the two companion papers of this project [*Xavier et al*., 2015; *Klingaman et al*., 2015a, 2015b], a strong link between them is generally not apparent based on several models which have participated in both the climate simulation and hindcast components of this project. For example, while the two NCAR GCMs, i.e., CAM5 and CAM5-ZM, only show moderate MJO performances in climate simulations as illustrated in Figures 3–6, these two models are among the top models in term of predictive skill for the two MJO events during the YOTC period [*Klingaman et al.*, 2015a]. However, note that model skill for the MJO in climate simulations is mainly evaluated by analyzing rainfall fields in this study; comprehensive evaluation of a model MJO performance will also need to examine circulation and outgoing longwave radiation patterns as suggested by *Crueger et al*. [2013]. Meanwhile, a more reliable model MJO predictive skill may also need to be evaluated based on a larger sample size of MJO events. More detailed analyses and discussions on the relationship between MJO fidelity in the 20 day hindcasts and 20 year climate simulations are provided by *Klingaman et al.* [2015b], which synthesizes the three components of the entire project.

While only results from limited analyses are presented in this study, one of the main purposes of this paper is to motivate further investigations on the key processes for the MJO by fully exploiting the data archive made available through this project, which can be publically accessed through the website: https://earthsystemcog.org/projects/gass-yotc-mip/. Also noteworthy is that in considering the global coverage for many variables archived from model integrations, particularly from models participating in the climate simulation component, these data should not be limited only for tropical studies but are also valuable for studies on subtropical and middle to high-latitude processes.

Acknowledgments
The multimodel output collected by this project and analyzed in this study is available for free download from https://earthsystemcog.org/projects/gassyotc-mip/. We acknowledge the insightful comments from the Editor, C. Zhang, and J. Lin and other two reviewers, which greatly helped improve this manuscript. We would like to thank E. Maloney and J. Benedict for their help with the calculation of gross moist stability. We are indebted to E. Maloney, A. Del Genio, B. Wang, B. Mapes, M. Moncrieff, A. Majda, C. Zhang, T. Li, and WGNE MJO Task Force members for stimulating discussions during the course of this study. X. Jiang acknowledges support by National Science Foundation (NSF) Climate and Large-Scale Dynamics Program under awards AGS-1228302, and NOAA MAPP program under award NA12OAR4310075. D. Waliser acknowledges the Office of Naval Research under Project ONRBAA12-001, NSF AGS-1221013, and the Jet Propulsion Laboratory, California Institute of Technology, under a contract with the NASA. N. Klingaman and S. Woolnough were supported by the National Centre for Atmospheric Science, a National Environment Research Council collaborative center, under contract R8/H12/83/001. P. Xavier and J. Petch are supported by the Joint DECC/Defra Met Office Hadley Centre Climate Programme (GA01101). D. Kim was supported by the NASA grant NNX13AM18G and the Korea Meteorological Administration Research and Development Program under grant CATER 2013–3142, and he appreciates the NASA/GISS modeling group, especially M. Kelley, M.-S. Yao, and A. Del Genio for their invaluable and unlimited supports. J. Ridout gratefully acknowledges support from the Office of Naval Research Program Element 0601153N, a grant of computing time from the United States Department of Defense High Performance Computing Modernization Program. The SMHI simulations were performed on resources provided by the Swedish National Infrastructure for Computing (SNIC) at the Parallel Computing Centre (PDC). The National Center for Atmospheric Research is sponsored by the National Science Foundation. Some of this research by T. Crueger has received funding from the European Union, Seventh Framework Programme (FP7/2007-2013) under grant agreement 244067. The effort of H.-Y. Ma was funded by the RGCM and ASR programs of the U.S. DOE as part of the CAPT. This work was performed under the auspices of the U.S. DOE by LLNL under contract DE-AC52-07NA27344. C. Stan was supported by NSF grant AGS-1211848. K.-H. Seo is supported by the National

References

Andersen, J. A., and Z. Kuang (2012), Moist static energy budget of MJO-like disturbances in the atmosphere of a zonally symmetric aquaplanet, *J. Clim.*, *25*, 2782–2804.

Annamalai, H., and K. R. Sperber (2005), Regional heat sources and the active and break phases of boreal summer intraseasonal (30–50 day) variability, *J. Atmos. Sci.*, *62*, 2726–2748.

Bao, Q., et al., (2013), The flexible global ocean-atmosphere-land system model, spectral version 2: FGOALS-s2, *Adv. Atmos. Sci.*, *30*, 561–576, doi:10.1007/s00376-012-2113-9.

Bechtold, P., M. Kohler, T. Jung, F. Doblas-Reyes, M. Leutbecher, M. J. Rodwell, F. Vitart, and G. Balsamo (2008), Advances in simulating atmospheric variability with the ECMWF model: From synoptic to decadal time-scales, *Q. J. R. Meteorol. Soc.*, *134*, 1337–1351.

Benedict, J. J., and D. A. Randall (2007), Observed characteristics of the MJO relative to maximum rainfall, *J. Atmos. Sci.*, *64*, 2332–2354.

Benedict, J. J., and D. A. Randall (2009), Structure of the Madden-Julian oscillation in the superparameterized CAM, *J. Atmos. Sci.*, *66*, 3277–3296.

Benedict, J. J., E. D. Maloney, A. H. Sobel, D. M. Frierson, and L. J. Donner (2013), Tropical intraseasonal variability in version 3 of the GFDL atmosphere model, *J. Clim.*, *26*, 426–449.

Benedict, J. J., E. D. Maloney, A. H. Sobel, and D. M. W. Frierson (2014), Gross moist stability and MJO simulation skill in three full-physics GCMs, *J. Atmos. Sci.*, *71*, 3327–3349.

Berg, W., T. L'Ecuyer, and J. M. Haynes (2010), The distribution of rainfall over oceans from spaceborne radars, *J. Appl. Meteorol. Climatol.*, *49*, 535–543.

Bessafi, M., and M. C. Wheeler (2006), Modulation of south Indian ocean tropical cyclones by the Madden-Julian oscillation and convectively coupled equatorial waves, *Mon. Weather Rev.*, *134*, 638–656.

Bollasina, M., and Y. Ming (2013), The general circulation model precipitation bias over the southwestern equatorial Indian Ocean and its implications for simulating the South Asian monsoon, *Clim. Dyn.*, *40*, 823–838.

Bony, S., and K. A. Emanuel (2005), On the role of moist processes in tropical intraseasonal variability: Cloud-radiation and moisture-convection feedbacks, *J. Atmos. Sci.*, *62*, 2770–2789.

Boyle, J., S. Klein, G. Zhang, S. Xie, and X. Wei (2008), Climate model forecast experiments for TOGA COARE, *Mon. Weather Rev.*, *136*, 808–832.

Bretherton, C. S., M. E. Peters, and L. E. Back (2004), Relationships between water vapor path and precipitation over the tropical oceans, *J. Clim.*, *17*, 1517–1528.

Brown, A., S. Milton, M. Cullen, B. Golding, J. Mitchell, and A. Shelly (2012), Unified modeling and prediction of weather and climate: A 25-year journey, *Bull. Am. Meteorol. Soc.*, *93*, 1865–1877.

Cai, Q., G. J. Zhang, and T. Zhou (2013), Impacts of shallow convection on MJO simulation: A moist static energy and moisture budget analysis, *J. Clim.*

Cassou, C. (2008), Intraseasonal interaction between the Madden-Julian oscillation and the North Atlantic Oscillation, *Nature*, *455*, 523–527.

Chen, Y. H., and A. D. Del Genio (2009), Evaluation of tropical cloud regimes in observations and a general circulation model, *Clim. Dyn.*, *32*, 355–369.

Chikira, M., and M. Sugiyama (2010), A cumulus parameterization with state-dependent entrainment rate. Part I: Description and sensitivity to temperature and humidity profiles, *J. Atmos. Sci.*, *67*, 2171–2193.

Côté, J., S. Gravel, A. Méthot, A. Patoine, M. Roch, and A. Staniforth (1998), The operational CMC-MRB Global Environmental Multiscale (GEM) model. Part I: Design considerations and formulation, *Mon. Weather Rev.*, *126*, 1373–1395.

Crueger, T., B. Stevens, and R. Brokopf (2013), The Madden-Julian oscillation in ECHAM6 and the introduction of an objective MJO metric, *J. Clim.*, *26*, 3241–3257.

Dee, D. P., et al. (2011), The ERA-Interim reanalysis: Configuration and performance of the data assimilation system, *Q. J. R. Meteorol. Soc.*, *137*, 553–597.

Del Genio, A. D., Y. Chen, D. Kim, and M.-S. Yao (2012), The MJO transition from shallow to deep convection in CloudSat/CALIPSO data and GISS GCM simulations, *J. Clim.*, *25*, 3755–3770.

DeMott, C. A., C. Stan, D. A. Randall, J. L. Kinter, and M. Khairoutdinov (2011), The Asian monsoon in the superparameterized CCSM and its relationship to tropical wave activity, *J. Clim.*, *24*, 5134–5156.

DeMott, C. A., C. Stan, D. A. Randall, and M. D. Branson (2014), Intraseasonal variability in coupled GCMs: The roles of ocean feedbacks and model physics, *J. Clim.*, *27*, 4970–4995.

Research Foundation of Korea grant (2011–0015486) funded by the Ministry of Education, Science and Technology. X. Wu is supported by the NSF under grant ATM-0935263. T. Miyakawa acknowledges M. Watanabe and N. Hirota for their support in providing MIROC data set, and the Earth Simulator (JIMSTEC) for the computation. W-L Tseng was supported by the German BMBF NORDATLANTIK project, and the Norddeutscher Verbund für Hoch- und Höchstleistungsrechnen for the computation.

Deng, L., and X. Wu (2010), Effects of convective processes on GCM simulations of the Madden-Julian oscillation, *J. Clim.*, *23*, 352–377.
Deng, L., and X. Wu (2011), Physical mechanisms for the maintenance of GCM-simulated Madden-Julian oscillation over the Indian Ocean and Pacific, *J. Clim.*, *24*, 2469–2482.
Ding, R. Q., J. P. Li, and K. H. Seo (2010), Predictability of the Madden-Julian oscillation estimated using observational data, *Mon. Weather Rev.*, *138*, 1004–1013.
Emanuel, K. A. (1987), An air-sea interaction-model of intraseasonal oscillations in the tropics, *J. Atmos. Sci.*, *44*, 2324–2340.
Forbes, R., A. Tompkins, and A. Untch (2012), A new prognostic bulk microphysics scheme for the IFS. *ECMWF Tech Memo* 649.
Fu, X. H., and B. Wang (2009), Critical roles of the stratiform rainfall in sustaining the Madden-Julian oscillation: GCM experiments, *J. Clim.*, *22*, 3939–3959.
Gill, A. E. (1980), Some simple solutions for heat-induced tropical circulation, *Q. J. R. Meteorol. Soc.*, *106*, 447–462.
Gottschalck, J., et al. (2010), A framework for assessing operational Madden-Julian oscillation forecasts: A CLIVAR MJO working group project, *Bull. Am. Meteorol. Soc.*, *91*, 1247–1258.
Guan, B., D. E. Waliser, N. P. Molotch, E. J. Fetzer, and P. J. Neiman (2012), Does the Madden-Julian oscillation influence wintertime atmospheric rivers and snowpack in the Sierra Nevada?, *Mon. Weather Rev.*, *140*, 325–342.
Guo, Y., X. Jiang, and D. E. Waliser (2014), Modulation of the convectively coupled Kelvin waves over South America and the tropical Atlantic Ocean in association with the Madden-Julian oscillation, *J. Atmos. Sci.*, *71*, 1371–1388.
Guo, Y., D. E. Waliser, and X. Jiang (2015), A systematic relationship between the representations of convectively coupled equatorial wave activity and the Madden-Julian oscillation in climate model simulations, *J. Clim.*, *28*, 1881–1904.
Hagos, S., L. R. Leung, and J. Dudhia (2011), Thermodynamics of the Madden-Julian oscillation in a regional model with constrained moisture, *J. Atmos. Sci.*, *68*, 1974–1989.
Han, Y., and B. Khouider (2010), Convectively coupled waves in a sheared environment, *J. Atmos. Sci.*, *67*, 2913–2942.
Hannah, W. M., and E. D. Maloney (2011), The role of moisture-convection feedbacks in simulating the Madden-Julian oscillation, *J. Clim.*, *24*, 2754–2770.
Harshvardhan, R. Davies, D. A. Randall, and T. G. Corsetti (1987), A fast radiation parameterization for atmospheric circulation models, *J. Geophys. Res.*, *92*, 1009–1016, doi:10.1029/JD092iD01p01009.
Hazeleger, W., et al. (2012), EC-Earth V2.2: Description and validation of a new seamless Earth system prediction model, *Clim. Dyn.*, *39*, 2611–2629.
Hendon, H. H., M. C. Wheeler, and C. D. Zhang (2007), Seasonal dependence of the MJO-ENSO relationship, *J. Clim.*, *20*, 531–543.
Hogan, T. F., et al. (2014), The navy global environmental model, *Oceanography*, *27*, 64–74.
Holloway, C. E., and J. D. Neelin (2009), Moisture vertical structure, column water vapor, and tropical deep convection, *J. Atmos. Sci.*, *66*, 1665–1683.
Holloway, C. E., S. J. Woolnough, and G. M. S. Lister (2013), The effects of explicit versus parameterized convection on the MJO in a large-domain high-resolution tropical case study. Part I: Characterization of large-scale organization and propagation*, *J. Atmos. Sci.*, *70*, 1342–1369.
Houze, R. A. (1982), Cloud clusters and large-scale vertical motions in the tropics, *J. Meteorol. Soc. Jpn.*, *60*, 396–410.
Hsu, P. C., and T. Li (2012), Role of the boundary layer moisture asymmetry in causing the eastward propagation of the Madden-Julian oscillation, *J. Clim.*, *25*, 4914–4931.
Huffman, G. J., R. F. Adler, B. Rudolf, U. Schneider, and P. R. Keehn (1995), Global precipitation estimates based on a technique for combining satellite-based estimates, rain-gauge analysis, and NWP model precipitation information, *J. Clim.*, *8*, 1284–1295.
Hung, M.-P., J.-L. Lin, W. Wang, D. Kim, T. Shinoda, and S. J. Weaver (2013), MJO and convectively coupled equatorial waves simulated by CMIP5 climate models, *J. Clim.*, *26*, 6185–6214.
Hurrell, J., G. A. Meehl, D. Bader, T. L. Delworth, B. Kirtman, and B. Wielicki (2009), A unified modeling approach to climate system prediction, *Bull. Am. Meteorol. Soc.*, *90*, 1819–1832.
Inness, P. M., and J. M. Slingo (2003), Simulation of the Madden-Julian oscillation in a coupled general circulation model. Part I: Comparison with observations and an atmosphere-only GCM, *J. Clim.*, *16*, 345–364.
Inness, P. M., J. M. Slingo, E. Guilyardi, and J. Cole (2003), Simulation of the Madden-Julian oscillation in a coupled general circulation model. Part II: The role of the basic state, *J. Clim.*, *16*, 365–382.
Jiang, X., et al. (2009), Vertical heating structures associated with the MJO as characterized by TRMM estimates, ECMWF reanalyses, and forecasts: A case study during 1998/99 winter, *J. Clim.*, *22*, 6001–6020.
Jiang, X., D. E. Waliser, W. S. Olson, W.-K. Tao, T. S. L'Ecuyer, K.-F. Li, Y. L. Yung, S. Shige, S. Lang, and Y. N. Takayabu (2011), Vertical diabatic heating structure of the MJO: Intercomparison between recent reanalyses and TRMM estimates, *Mon. Weather Rev.*, *139*, 3208–3223.
Jiang, X., M. Zhao, and D. E. Waliser (2012), Modulation of tropical cyclones over the eastern Pacific by the intraseasonal variability simulated in an AGCM, *J. Clim.*, *25*, 6524–6538.
Johnson, R. H., T. M. Rickenbach, S. A. Rutledge, P. E. Ciesielski, and W. H. Schubert (1999), Trimodal characteristics of tropical convection, *J. Clim.*, *12*, 2397–2418.
Johnson, R. H., P. E. Ciesielski, J. H. Ruppert, and M. Katsumata (2014), Sounding-based thermodynamic budgets for DYNAMO, *J. Atmos. Sci.*, *72*, 598–622.
Katsumata, M., R. H. Johnson, and P. E. Ciesielski (2009), Observed synoptic-scale variability during the developing phase of an ISO over the Indian Ocean during MISMO, *J. Atmos. Sci.*, *66*, 3434–3448.
Kemball-Cook, S., and B. Wang (2001), Equatorial waves and air-sea interaction in the boreal summer intraseasonal oscillation, *J. Clim.*, *14*, 2923–2942.
Kemball-Cook, S. R., and B. C. Weare (2001), The onset of convection in the Madden-Julian oscillation, *J. Clim.*, *14*, 780–793.
Kessler, W. S., and R. Kleeman (2000), Rectification of the Madden-Julian oscillation into the ENSO cycle, *J. Clim.*, *13*, 3560–3575.
Khairoutdinov, M., C. DeMott, and D. Randall (2008), Evaluation of the simulated interannual and subseasonal variability in an AMIP-style simulation using the CSU multiscale modeling framework, *J. Clim.*, *21*, 413–431.
Khouider, B., and A. J. Majda (2006), A simple multicloud parameterization for convectively coupled tropical waves. Part I: Linear analysis, *J. Atmos. Sci.*, *63*, 1308–1323.
Khouider, B., Y. Han, A. J. Majda, and S. N. Stechmann (2012), Multiscale waves in an MJO background and convective momentum transport feedback, *J. Atmos. Sci.*, *69*, 915–933.
Kikuchi, K., and Y. N. Takayabu (2004), The development of organized convection associated with the MJO during TOGA COARE IOP: Trimodal characteristics, *Geophys. Res. Lett.*, *31*, L10101, doi:10.1029/2004GL019601.
Kiladis, G. N., K. H. Straub, and P. T. Haertel (2005), Zonal and vertical structure of the Madden-Julian oscillation, *J. Atmos. Sci.*, *62*, 2790–2809.

Kiladis, G. N., M. C. Wheeler, P. T. Haertel, K. H. Straub, and P. E. Roundy (2009), Convectively coupled equatorial waves, *Rev. Geophys.*, *47*, RG2003, doi:10.1029/2008RG000266.

Kim, D., et al. (2009), Application of MJO simulation diagnostics to climate models, *J. Clim.*, *22*, 6413–6436.

Kim, D., A. H. Sobel, E. D. Maloney, D. M. W. Frierson, and I. S. Kang (2011), A systematic relationship between intraseasonal variability and mean state bias in AGCM simulations, *J. Clim.*, *24*, 5506–5520.

Kim, D., A. H. Sobel, A. D. Del Genio, Y. Chen, S. J. Camargo, M.-S. Yao, M. Kelley, and L. Nazarenko (2012), The tropical subseasonal variability simulated in the NASA GISS general circulation model, *J. Clim.*, *25*, 4641–4659.

Kim, D., J.-S. Kug, and A. H. Sobel (2014a), Propagating versus nonpropagating Madden-Julian oscillation events, *J. Clim.*, *27*, 111–125.

Kim, D., et al. (2014b), Process-oriented MJO simulation diagnostic: Moisture sensitivity of simulated convection, *J. Clim.*, *27*, 5379–5395.

Klingaman, N. P., and S. J. Woolnough (2014), The role of air-sea coupling in the simulation of the Madden-Julian oscillation in the Hadley Centre model, *Q. J. R. Meteorol. Soc.*, *140*, 2272–228.

Klingaman, N. P., et al. (2015a), Vertical structure and physical processes of the Madden-Julian oscillation: Linking hindcast fidelity to simulated diabatic heating and moistening, *J. Geophys. Res. Atmos.*, *120*, doi:10.1002/2014JD022374.

Klingaman, N. P., X. Jiang, P. K. Xavier, J. Petch, D. Waliser, and S. J. Woolnough (2015b), Vertical structure and physical processes of the Madden-Julian oscillation: Synthesis and summary, *J. Geophys. Res. Atmos.*, *120*, doi:10.1002/2015JD023196.

Klotzbach, P. J. (2010), On the Madden-Julian oscillation-Atlantic hurricane relationship, *J. Clim.*, *23*, 282–293.

Kuang, Z. (2008), A moisture-stratiform instability for convectively coupled waves, *J. Atmos. Sci.*, *65*, 834–854.

Lappen, C.-L., and C. Schumacher (2012), Heating in the tropical atmosphere: What level of detail is critical for accurate MJO simulations in GCMs?, *Clim. Dyn.*, *39*, 2547–2568.

Lappen, C.-L., and C. Schumacher (2014), The role of tilted heating in the evolution of the MJO, *J. Geophys. Res. Atmos.*, *119*, 2966–2989, doi:10.1002/2013JD020638.

Lau, K. M., H. T. Wu, Y. C. Sud, and G. K. Walker (2005), Effects of cloud microphysics on tropical atmospheric hydrologic processes and intraseasonal variability, *J. Clim.*, *18*, 4731–4751.

Lau, K.-M., and P. H. Chan (1986), Aspects of the 40–50 day oscillation during the northern summer as inferred from outgoing longwave radiation, *Mon. Weather Rev.*, *114*, 1354–1367.

Lau, W. K.-M., and D. E. Waliser (2012), *Intraseasonal Variability in the Atmosphere-Ocean Climate System*, 2nd ed., 613 pp., Springer, Heidelberg, Germany.

Lee, M. I., I. S. Kang, J. K. Kim, and B. E. Mapes (2001), Influence of cloud-radiation interaction on simulating tropical intraseasonal oscillation with an atmospheric general circulation model, *J. Geophys. Res.*, *106*, 14,219–14,233, doi:10.1029/2001JD900143.

L'Heureux, M. L., and R. W. Higgins (2008), Boreal winter links between the Madden-Julian oscillation and the Arctic Oscillation, *J. Clim.*, *21*, 3040–3050.

Li, C. Y., X. L. Jia, J. Ling, W. Zhou, and C. D. Zhang (2009), Sensitivity of MJO simulations to diabatic heating profiles, *Clim. Dyn.*, *32*, 167–187.

Liebmann, B., H. H. Hendon, and J. D. Glick (1994), The relationship between tropical cyclones of the western Pacific and Indian Oceans and the Madden-Julian oscillation, *J. Meteorol. Soc. Jpn.*, *72*, 401–412.

Lin, H., G. Brunet, and J. Derome (2009), An observed connection between the North Atlantic Oscillation and the Madden-Julian oscillation, *J. Clim.*, *22*, 364–380.

Lin, J. L., and B. E. Mapes (2004), Radiation budget of the tropical intraseasonal oscillation, *J. Atmos. Sci.*, *61*, 2050–2062.

Lin, J. L., D. Kim, M. I. Lee, and I. S. Kang (2007), Effects of cloud-radiative heating on atmospheric general circulation model (AGCM) simulations of convectively coupled equatorial waves, *J. Geophys. Res.*, *112*, D24107, doi:10.1029/2006JD008291.

Lin, J., B. Mapes, M. Zhang, and M. Newman (2004), Stratiform precipitation, vertical heating profiles, and the Madden-Julian oscillation, *J. Atmos. Sci.*, *61*, 296–309.

Lin, J.-L., et al. (2006), Tropical intraseasonal variability in 14 IPCC AR4 climate models. Part I: Convective signals, *J. Clim.*, *19*, 2665–2690.

Ling, J., and C. Zhang (2011), Structural evolution in heating profiles of the MJO in global reanalyses and TRMM retrievals, *J. Clim.*, *24*, 825–842.

Liou, C. S., J. H. Chen, C. T. Terng, F. J. Wang, C. T. Fong, T. E. Rosmond, H. C. Kuo, C. H. Shiao, and M. D. Cheng (1997), The second–generation global forecast system at the central weather bureau in Taiwan, *Weather Forecasting*, *12*, 653–663, doi:10.1175/1520-0434-12.3.653.

Lorenz, D. J., and D. L. Hartmann (2006), The effect of the MJO on the North American monsoon, *J. Clim.*, *19*, 333–343.

Ma, D., and Z. M. Kuang (2011), Modulation of radiative heating by the Madden-Julian oscillation and convectively coupled Kelvin waves as observed by CloudSat, *Geophys. Res. Lett.*, *38*, L21813, doi:10.1029/2011GL049734.

Ma, H. Y., S. Xie, J. S. Boyle, S. A. Klein, and Y. Zhang (2013), Metrics and diagnostics for precipitation-related processes in climate model short-range hindcasts, *J. Clim.*, *26*, 1516–1534.

Madden, R. A., and P. R. Julian (1971), Detection of a 40–50 day oscillation in zonal wind in tropical Pacific, *J. Atmos. Sci.*, *28*, 702–708.

Madden, R. A., and P. R. Julian (1972), Description of global-scale circulation cells in tropics with a 40–50 day period, *J. Atmos. Sci.*, *29*, 1109–1123.

Majda, A. J., and J. A. Biello (2004), A multiscale model for tropical intraseasonal oscillations, *Proc. Natl. Acad. Sci. U. S. A.*, *101*, 4736–4741.

Majda, A. J., and S. N. Stechmann (2009), A simple dynamical model with features of convective momentum transport, *J. Atmos. Sci.*, *66*, 373–392.

Maloney, E. D. (2009), The moist static energy budget of a composite tropical intraseasonal oscillation in a climate model, *J. Clim.*, *22*, 711–729.

Maloney, E. D., and A. H. Sobel (2004), Surface fluxes and ocean coupling in the tropical intraseasonal oscillation, *J. Clim.*, *17*, 4368–4386.

Maloney, E. D., and D. L. Hartmann (1998), Frictional moisture convergence in a composite life cycle of the Madden-Julian oscillation, *J. Clim.*, *11*, 2387–2403.

Maloney, E. D., and D. L. Hartmann (2000), Modulation of eastern North Pacific hurricanes by the Madden-Julian oscillation, *J. Clim.*, *13*, 1451–1460.

Maloney, E. D., A. H. Sobel, and W. M. Hannah (2010), Intraseasonal variability in an aquaplanet general circulation model, *J. Adv. Model. Earth Syst.*, *2*, 24, doi:10.3894/JAMES.2010.2.5.

Maloney, E., X. Jiang, S.-P. Xie, and J. Benedict (2014), Process-oriented diagnosis of East Pacific warm pool intraseasonal variability, *J. Clim.*, *27*, 6305–6324.

Mapes, B. E. (2000), Convective inhibition, subgrid-scale triggering energy, and stratiform instability in a toy tropical wave model, *J. Atmos. Sci.*, *57*, 1515–1535.

Matthews, A. J. (2008), Primary and successive events in the Madden-Julian oscillation, *Q. J. R. Meteorol. Soc.*, *134*, 439–453.

McPhaden, M. J. (1999), Genesis and evolution of the 1997–98 El Nino, *Science*, *283*, 950–954.

Merryfield, W. J., W.-S. Lee, G. J. Boer, V. V. Kharin, J. F. Scinocca, G. M. Flato, R. S. Ajayamohan, J. C. Fyfe, Y. Tang, and S. Polavarapu (2013), The Canadian seasonal to interannual prediction system. Part I: Models and initialization, *Mon. Weather Rev.*, *141*, 2910–2945.

Miyakawa, T., Y. N. Takayabu, T. Nasuno, H. Miura, M. Satoh, and M. W. Moncrieff (2012), Convective momentum transport by rainbands within a Madden-Julian oscillation in a global nonhydrostatic model with explicit deep convective processes. Part I: Methodology and general results, *J. Atmos. Sci.*, *69*, 1317–1338.

Molod, A., L. Takacs, L. M. Suarez, J. Bacmeister, I.-S. Song, and A. Eichmann (2012), The GEOS-5 atmospheric general circulation model: Mean climate and development from MERRA to Fortuna, *NASA Technical Report Series on Global Modeling and Data Assimilation*, *NASA TM-2012-104606*, Vol. 28, 117 pp.

Moncrieff, M. W., D. E. Waliser, M. J. Miller, M. A. Shapiro, G. R. Asrar, and J. Caughey (2012), Multiscale convective organization and the YOTC virtual global field campaign, *Bull. Am. Meteorol. Soc.*, *93*, 1171–1187.

Morcrette, J. J., H. W. Barker, J. N. S. Cole, M. J. Iacono, and R. Pincus (2008), Impact of a new radiation package, McRad, in the ECMWF integrated forecasting system, *Mon. Weather Rev.*, *136*, 4773–4798.

Morita, J., Y. N. Takayabu, S. Shige, and Y. Kodama (2006), Analysis of rainfall characteristics of the Madden-Julian oscillation using TRMM satellite data, *Dyn. Atmos. Oceans*, *42*, 107–126.

Nakazawa, T. (1988), Tropical super clusters within intraseasonal variations over the western Pacific, *J. Meteorol. Soc. Jpn.*, *66*, 823–839.

National Academy of Sciences (2010), Assessment of Intraseasonal to Interannual Climate Prediction and Predictability.

Neale, R. B., et al. (2012), Description of the NCAR Community Atmosphere Model:CAM 5.0, *Tech. Rep. NCAR/TN-486+STR*, National Center for Atmospheric Research, Boulder, Colorado.

Neelin, J. D., and I. M. Held (1987), Modeling tropical convergence based on the moist static energy budget, *Mon. Weather Rev.*, *115*, 3–12.

Neelin, J. D., I. M. Held, and K. H. Cook (1987), Evaporation-wind feedback and low-frequency variability in the tropical atmosphere, *J. Atmos. Sci.*, *44*, 2341–2348.

Neena, J. M., J. Y. Lee, D. Waliser, B. Wang, and X. Jiang (2014), Predictability of the Madden-Julian oscillation in the Intraseasonal Variability Hindcast Experiment (ISVHE), *J. Clim.*, *27*, 4531–4543.

Oh, J. H., K. Y. Kim, and G. H. Lim (2012), Impact of MJO on the diurnal cycle of rainfall over the western Maritime Continent in the austral summer, *Clim. Dyn.*, *38*, 1167–1180.

Oh, J. H., X. Jiang, D. Waliser, M. Moncrieff, and R. Johnson (2015), Convective momentum transport associated with the Madden-Julian oscillation based on a reanalysis dataset, *J. Clim.*, doi:10.1175/JCLI-D-14-00570.1, in press.

Petch, J., D. Waliser, X. Jiang, P. Xavier, and S. Woolnough (2011), A global model inter-comparison of the physical processes associated with the MJO, *GEWEX News*, August.

Peters, O., and J. D. Neelin (2006), Critical phenomena in atmospheric precipitation, *Nat. Phys.*, *2*, 393–396.

Phillips, T. J., G. L. Potter, D. L. Williamson, R. T. Cederwall, J. S. Boyle, M. Fiorino, J. J. Hnilo, J. G. Olson, S. Xie, and J. J. Yio (2004), Evaluating parameterizations in general circulation models: Climate simulation meets weather prediction, *Bull. Am. Meteorol. Soc.*, *85*, 1903–1915.

Pritchard, M. S., and C. S. Bretherton (2014), Causal evidence that rotational moisture advection is critical to the superparameterized Madden-Julian oscillation, *J. Atmos. Sci.*, *71*, 800–815.

Randall, D., M. Khairoutdinov, A. Arakawa, and W. Grabowski (2003), Breaking the cloud parameterization deadlock, *Bull. Am. Meteorol. Soc.*, *84*, 1547–1564.

Rashid, H. A., H. H. Hendon, M. C. Wheeler, and O. Alves (2011), Prediction of the Madden-Julian oscillation with the POAMA dynamical prediction system, *Clim. Dyn.*, *36*, 649–661.

Rauniyar, S. P., and K. J. E. Walsh (2011), Scale interaction of the diurnal cycle of rainfall over the Maritime Continent and Australia: Influence of the MJO, *J. Clim.*, *24*, 325–348.

Raymond, D. J. (2001), A new model of the Madden-Julian oscillation, *J. Atmos. Sci.*, *58*, 2807–2819.

Raymond, D. J., and Ž. Fuchs (2009), Moisture modes and the Madden-Julian oscillation, *J. Clim.*, *22*, 3031–3046.

Raymond, D. J., S. Sessions, A. Sobel, and Z. Fuchs (2009), The mechanics of gross moist stability, *J. Adv. Model. Earth Syst.*, *1*, 20.

Reynolds, R. W., N. A. Rayner, T. M. Smith, D. C. Stokes, and W. Wang (2002), An improved in situ and satellite SST analysis for climate, *J. Clim.*, *15*, 1609–1625.

Ruppert, J. H., and R. H. Johnson (2014), Diurnally modulated cumulus moistening in the pre-onset stage of the Madden-Julian oscillation during DYNAMO, *J. Atmos. Sci.*, *72*, 1622–1647.

Saha, S., et al. (2006), The NCEP climate forecast system, *J. Clim.*, *19*, 3483–3517.

Saha, S., et al. (2013), The NCEP climate forecast system version 2, *J. Clim.*, *27*, 2185–2208.

Sahany, S., J. D. Neelin, K. Hales, and R. B. Neale (2012), Temperature-moisture dependence of the deep convective transition as a constraint on entrainment in climate models, *J. Atmos. Sci.*, *69*, 1340–1358.

Salby, M. L., H. H. Hendon, and R. R. Garcia (1994), Planetary-scale circulations in the presence of climatological and wave-induced heating, *J. Atmos. Sci.*, *51*, 3365–3365.

Schmidt, G. A., et al. (2014), Configuration and assessment of the GISS ModelE2 contributions to the CMIP5 archive, *J. Adv. Model. Earth Syst.*, *6*, 141–184, doi:10.1002/2013MS000265.

Schumacher, C., and R. A. Houze (2003), Stratiform rain in the tropics as seen by the TRMM precipitation radar, *J. Clim.*, *16*, 1739–1756.

Seo, K. H., and S. W. Son (2012), The global atmospheric circulation response to tropical diabatic heating associated with the Madden-Julian oscillation during northern winter, *J. Atmos. Sci.*, *69*, 79–96.

Seo, K. H., and W. Q. Wang (2010), The Madden-Julian oscillation simulated in the NCEP climate forecast system model: The importance of stratiform heating, *J. Clim.*, *23*, 4770–4793.

Seo, K.-H., W. Wang, J. Gottschalck, Q. Zhang, J.-K. E. Schemm, W. R. Higgins, and A. Kumar (2009), Evaluation of MJO forecast skill from several statistical and dynamical forecast models, *J. Clim.*, *22*, 2372–2388.

Serra, Y. L., X. Jiang, B. Tian, J. Amador Astua, E. D. Maloney, and G. N. Kiladis (2014), Tropical intra-seasonal modes of the atmosphere, *Ann. Rev. Environ. Resour.*, *39*, 189–215.

Slingo, J. M., and R. A. Madden (1991), Characteristics of the tropical intraseasonal oscillation in the NCAR community climate model, *Q. J. R. Meteorol. Soc.*, *117*, 1129–1169.

Sobel, A., and E. Maloney (2012), An idealized semi-empirical framework for modeling the Madden-Julian oscillation, *J. Atmos. Sci.*, *69*, 1691–1705.

Sobel, A., and E. Maloney (2013), Moisture modes and the eastward propagation of the MJO, *J. Atmos. Sci.*, *70*, 187–192.

Sobel, A. H., and H. Gildor (2003), A simple time-dependent model of SST hot spots, *J. Clim.*, *16*, 3978–3992.

Sobel, A. H., J. Nilsson, and L. M. Polvani (2001), The weak temperature gradient approximation and balanced tropical moisture waves, *J. Atmos. Sci.*, *58*, 3650–3665.

Sobel, A. H., E. D. Maloney, G. Bellon, and D. M. Frierson (2010), Surface fluxes and tropical intraseasonal variability: A reassessment, *J. Adv. Model. Earth Syst.*, *2*, 2, doi:10.3894/JAMES.2010.2.2.

Song, X., and G. J. Zhang (2011), Microphysics parameterization for convective clouds in a global climate model: Description and single-column model tests, *J. Geophys. Res.*, *116*, D02201, doi:10.1029/2010JD014833.

Song, X., and R. Yu (2004), Underestimated tropical stratiform precipitation in the National Center for Atmospheric Research (NCAR) Community Climate Model (CCM3), *Geophys. Res. Lett.*, *31*, L24101, doi:10.1029/2004GL021292.

Sperber, K. R. (2003), Propagation and the vertical structure of the Madden-Julian oscillation, *Mon. Weather Rev.*, *131*, 3018–3037.

Sperber, K. R., J. M. Slingo, and H. Annamalai (2000), Predictability and the relationship between subseasonal and interannual variability during the Asian summer monsoon, *Q. J. R. Meteorol. Soc.*, *126*, 2545–2574.

Sperber, K. R., S. Gualdi, S. Legutke, and V. Gayler (2005), The Madden-Julian oscillation in ECHAM4 coupled and uncoupled general circulation models, *Clim. Dyn.*, *25*, 117–140.

Stachnik, J. P., C. Schumacher, and P. E. Ciesielski (2013), Total heating characteristics of the ISCCP tropical and subtropical cloud regimes, *J. Clim.*, *26*, 7097–7116.

Stan, C., M. Khairoutdinov, C. A. DeMott, V. Krishnamurthy, D. M. Straus, D. A. Randall, J. L. Kinter, and J. Shukla (2010), An ocean-atmosphere climate simulation with an embedded cloud resolving model, *Geophys. Res. Lett.*, *37*, L01702, doi:10.1029/2009GL040822.

Stephens, G. L., P. J. Webster, R. H. Johnson, R. Engelen, and T. L'Ecuyer (2004), Observational evidence for the mutual regulation of the tropical hydrological cycle and tropical sea surface temperatures, *J. Clim.*, *17*, 2213–2224.

Stevens, B., et al. (2013), Atmospheric component of the MPI-M Earth System Model: ECHAM6, *J. Adv. Model. Earth Syst.*, *5*, 146–172, doi:10.1002/jame.20015.

Sugiyama, M. (2009), The moisture mode in the quasi-equilibrium tropical circulation model. Part I: Analysis based on the weak temperature gradient approximation, *J. Atmos. Sci.*, *66*, 1507–1523.

Sultan, B., S. Janicot, and A. Diedhiou (2003), The West African monsoon dynamics. Part I: Documentation of intraseasonal variability, *J. Clim.*, *16*, 3389–3406.

Takayabu, Y. N. (1994), Large-scale cloud disturbances associated with equatorial waves .1. Spectral features of the cloud disturbances, *J. Meteorol. Soc. Jpn.*, *72*, 433–449.

Takayabu, Y. N., T. Iguchi, M. Kachi, A. Shibata, and H. Kanzawa (1999), Abrupt termination of the 1997–98 El Nino in response to a Madden-Julian oscillation, *Nature*, *402*, 279–282.

Thayer-Calder, K., and D. A. Randall (2009), The role of convective moistening in the Madden-Julian oscillation, *J. Atmos. Sci.*, *66*, 3297–3312.

Tian, B., D. E. Waliser, E. J. Fetzer, and Y. L. Yung (2010), Vertical moist thermodynamic structure of the Madden-Julian oscillation in atmospheric infrared sounder retrievals: An update and a comparison to ECMWF Interim re-analysis, *Mon. Weather Rev.*, *138*, 4576–4582.

Tokioka, T., K. Yamazaki, A. Kitoh, and T. Ose (1988), The equatorial 30–60 day oscillation and the Arakawa-Schubert penetrative cumulus parameterization, *J. Meteorol. Soc. Jpn.*, *66*, 883–901.

Tromeur, E., and W. B. Rossow (2010), Interaction of tropical deep convection with the large-scale circulation in the MJO, *J. Clim.*, *23*, 1837–1853.

Tseng, W.-L., B.-J. Tsuang, N. Keenlyside, H.-H. Hsu, and C.-Y. Tu (2014), Resolving the upper-ocean warm layer improves the simulation of the Madden-Julian Oscillation, *Clim. Dyn.*, *44*(5-6), 1487–1503.

Tung, W. W., and M. Yanai (2002), Convective momentum transport observed during the TOGA COARE IOP. Part II: Case studies, *J. Atmos. Sci.*, *59*, 2535–2549.

Vecchi, G. A., and N. A. Bond (2004), The Madden-Julian oscillation (MJO) and northern high latitude wintertime surface air temperatures, *Geophys. Res. Lett.*, *31*, L24804, doi:10.1029/2011GL049881.

Virts, K. S., J. M. Wallace, M. L. Hutchins, and R. H. Holzworth (2013), Diurnal lightning variability over the Maritime Continent: Impact of low-level winds, cloudiness, and the MJO, *J. Atmos. Sci.*, *70*, 3128–3146.

Vitart, F., and F. Molteni (2010), Simulation of the Madden-Julian oscillation and its teleconnections in the ECMWF forecast system, *Q. J. R. Meteorol. Soc.*, *136*, 842–855.

Voldoire, A., et al. (2013), The CNRM-CM5.1 global climate model: Description and basic evaluation, *Clim. Dyn.*, *40*, 2091–2121.

Waliser, D. E. (2012), Predictability and forecasting, in *Intraseasonal Variability in the Atmosphere–Ocean Climate System*, edited by W. K. M. Lau and D. E. Waliser, Springer, Heidelberg, Germany.

Waliser, D. E., K. M. Lau, and J. H. Kim (1999), The influence of coupled sea surface temperatures on the Madden-Julian oscillation: A model perturbation experiment, *J. Atmos. Sci.*, *56*, 333–358.

Waliser, D. E., W. Stern, S. Schubert, and K. M. Lau (2003), Dynamic predictability of intraseasonal variability associated with the Asian summer monsoon, *Q. J. R. Meteorol. Soc.*, *129*, 2897–2925.

Waliser, D. E., et al. (2012), The "Year" of tropical convection (May 2008–April 2010): Climate variability and weather highlights, *Bull. Am. Meteorol. Soc.*, *93*, 1189–1218.

Waliser, D., et al. (2009), MJO simulation diagnostics, *J. Clim.*, *22*, 3006–3030.

Walters, D. N., et al. (2011), The Met Office Unified Model Global Atmosphere 3.0/3.1 and JULES Global Land 3.0/3.1 configurations, *Geosci. Model Dev.*, *4*, 919–941.

Wang, B., and T. M. Li (1994), Convective interaction with boundary-layer dynamics in the development of a tropical intraseasonal system, *J. Atmos. Sci.*, *51*, 1386–1400.

Wang, B., and X. S. Xie (1996), Low-frequency equatorial waves in vertically sheared zonal flow .1. Stable waves, *J. Atmos. Sci.*, *53*, 449–467.

Wang, W., M.-P. Hung, S. Weaver, A. Kumar, and X. Fu (2013), MJO prediction in the NCEP Climate Forecast System version 2, *Clim. Dyn.*, *42*(9-10), 2509–2520.

Watanabe, M., et al. (2010), Improved climate simulation by MIROC5: Mean states, variability, and climate sensitivity, *J. Clim.*, *23*, 6312–6335.

Wheeler, M. C., H. H. Hendon, S. Cleland, H. Meinke, and A. Donald (2009), Impacts of the Madden-Julian oscillation on Australian rainfall and circulation, *J. Clim.*, *22*, 1482–1498.

Wheeler, M., and G. N. Kiladis (1999), Convectively coupled equatorial waves: Analysis of clouds and temperature in the wavenumber-frequency domain, *J. Atmos. Sci.*, *56*, 374–399.

Wu, T., R. Yu, F. Zhang, Z. Wang, M. Dong, L. Wang, X. Jin, D. Chen, and L. Li (2010), The Beijing Climate Center atmospheric general circulation model: Description and its performance for the present-day climate, *Clim. Dyn.*, *34*, 123–147.

Wu, X., and L. Deng (2013), Comparison of moist static energy and budget between the GCM-simulated Madden-Julian oscillation and observations over the Indian Ocean and western Pacific, *J. Clim.*, *26*, 4981–4993.

Xavier, P. K., et al. (2015), Vertical structure and physical processes of the Madden-Julian Oscillation: Biases and uncertainties at short range, *J. Geophys. Res. Atmos.*, *120*, doi:10.1002/2014JD022718.

Xie, S. C., H. Y. Ma, J. S. Boyle, S. A. Klein, and Y. Y. Zhang (2012), On the correspondence between short- and long-time-scale systematic errors in CAM4/CAM5 for the year of tropical convection, *J. Clim.*, *25*, 7937–7955.

Yanai, M., S. Esbensen, and J.-H. Chu (1973), Determination of bulk properties of tropical cloud clusters from large-scale heat and moisture budgets, *J. Atmos. Sci.*, *30*, 611–627.

Yasunari, T. (1979), Cloudiness fluctuations associated with the Northern Hemisphere summer monsoon, *J. Meteorol. Soc. Jpn.*, *57*, 227–242.

Yasunari, T. (1980), A quasi-stationary appearance of 30- to 40-day period in the cloudiness fluctuations during the summer monsoon over India, *J. Meteorol. Soc. Jpn.*, *58*, 225–229.

Yukimoto, S., et al. (2012), A new global climate model of the Meteorological Research Institute: MRI-CGCM3 - Model description and basic performance -, *J. Meteorol. Soc. Jpn. Ser. II*, *90A*, 23–64.

Zhang, C. (2013), Madden-Julian oscillation: Bridging weather and climate, *Bull. Am. Meteorol. Soc.*, *94*, 1849–1870.

Zhang, C. D., M. Dong, S. Gualdi, H. H. Hendon, E. D. Maloney, A. Marshall, K. R. Sperber, and W. Q. Wang (2006), Simulations of the Madden-Julian oscillation in four pairs of coupled and uncoupled global models, *Clim. Dyn.*, *27*, 573–592.

Zhang, C. D., J. A. Ling, S. Hagos, W. K. Tao, S. Lang, Y. N. Takayabu, S. Shige, M. Katsumata, W. S. Olson, and T. L'Ecuyer (2010), MJO signals in latent heating: Results from TRMM retrievals, *J. Atmos. Sci.*, *67*, 3488–3508.

Zhang, G. J., and M. Mu (2005a), Effects of modifications to the Zhang-McFarlane convection parameterization on the simulation of the tropical precipitation in the National Center for Atmospheric Research Community Climate Model, version 3, *J. Geophys. Res.*, *110*, D09109, doi:10.1029/2004JD005617.

Zhang, G. J., and M. Mu (2005b), Simulation of the Madden-Julian oscillation in the NCAR CCM3 using a revised Zhang-McFarlane convection parameterization scheme, *J. Clim.*, *18*, 4046–4064.

Zhang, G. J., and X. L. Song (2009), Interaction of deep and shallow convection is key to Madden-Julian oscillation simulation, *Geophys. Res. Lett.*, *36*, L09708, doi:10.1029/2009GL037340.

Zhang, M., and M. A. Geller (1994), Selective excitation of tropical atmospheric waves in wave-CISK: The effect of vertical wind shear, *J. Atmos. Sci.*, *51*, 353–368.

Zhou, L., R. B. Neale, M. Jochum, and R. Murtugudde (2012), Improved Madden-Julian oscillations with improved physics: The impact of modified convection parameterizations, *J. Clim.*, *25*, 1116–1136.

Zhu, H. Y., H. Hendon, and C. Jakob (2009), Convection in a parameterized and superparameterized model and its role in the representation of the MJO, *J. Atmos. Sci.*, *66*, 2796–2811.

Zhu, H., H. Hendon, M. Dix, Z. Sun, G. Dietachmayer, and K. Puri (2013), Vertical structure and diabatic processes of the MJO, A global model inter-comparison Project: Preliminary results from ACCESS model, *CAWCR Res. Lett.*, *10*, 2034–2038.